

FIGURE 1 (a)

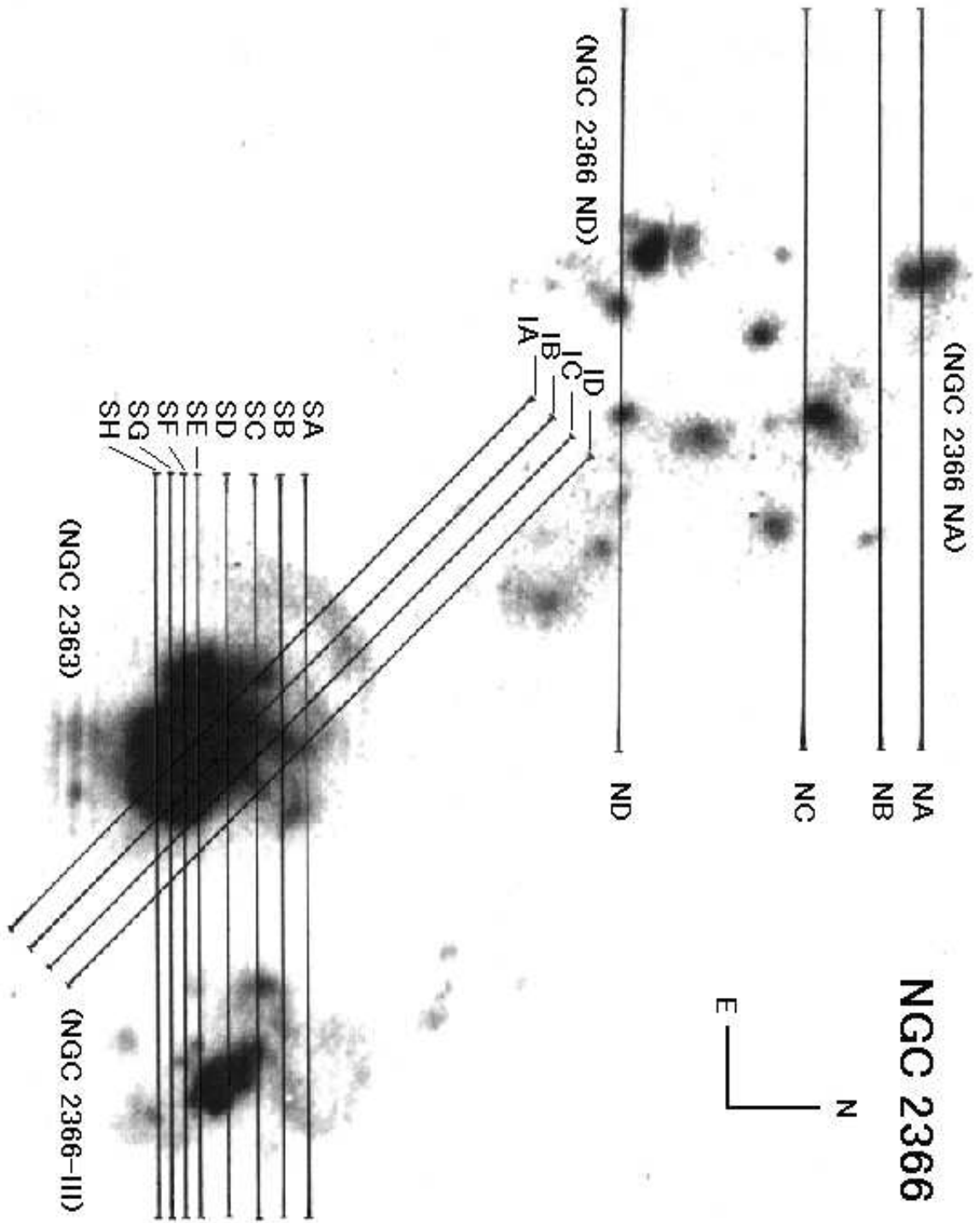


FIGURE 1 (b)

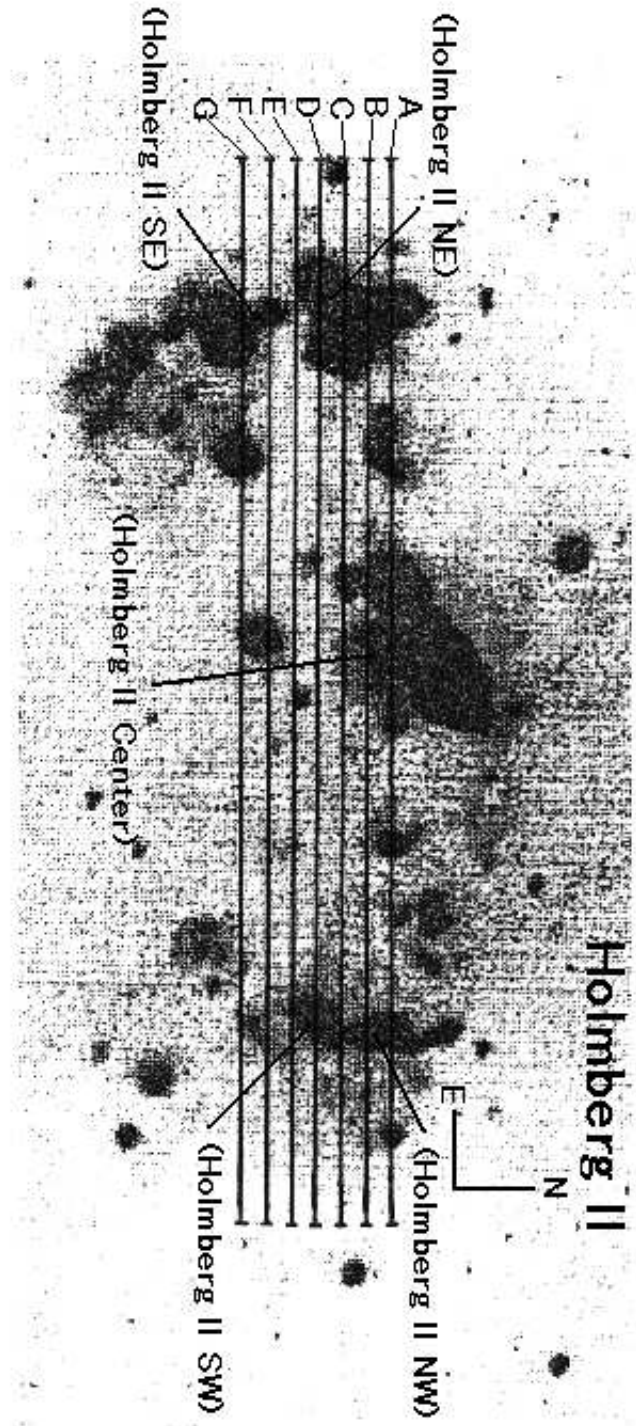


FIGURE 1 (c)

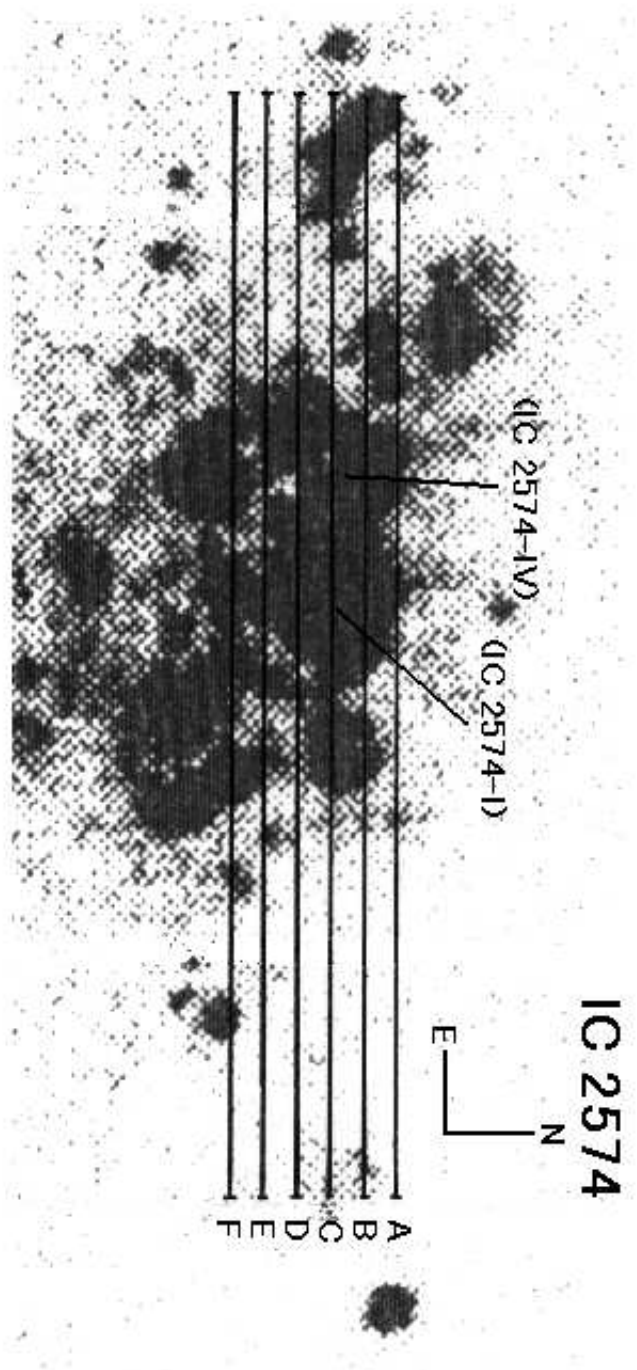


FIGURE 1 (d)

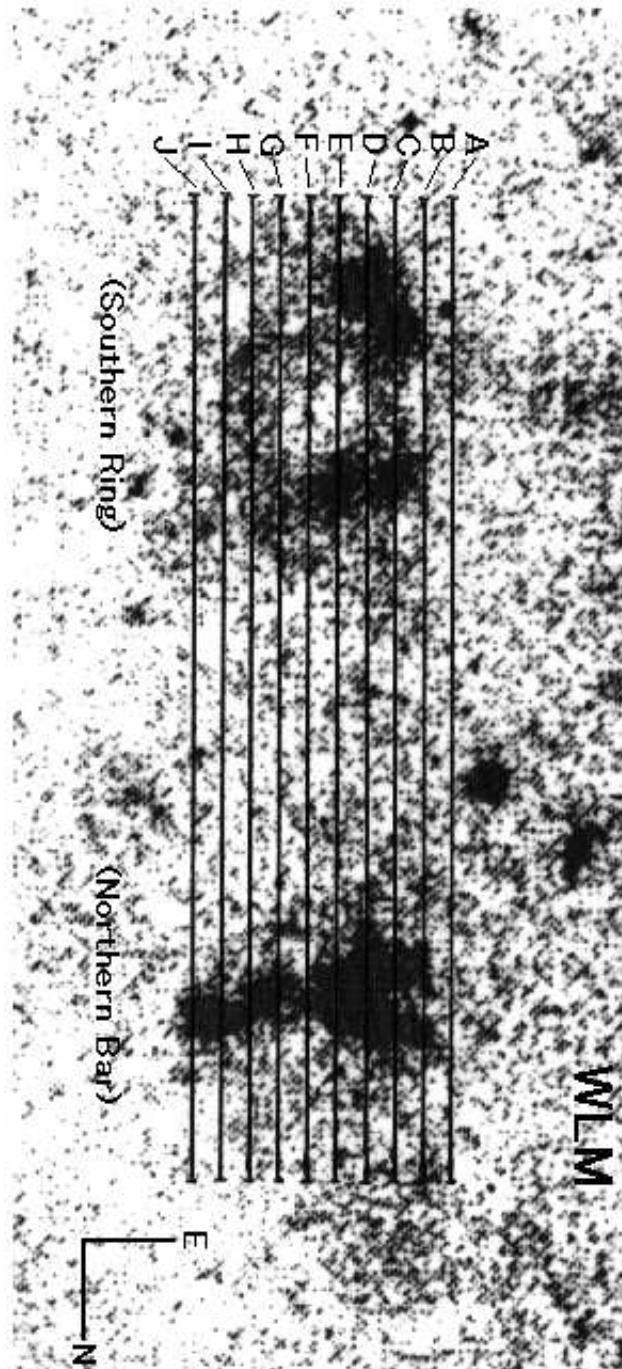


FIGURE 2 (a)

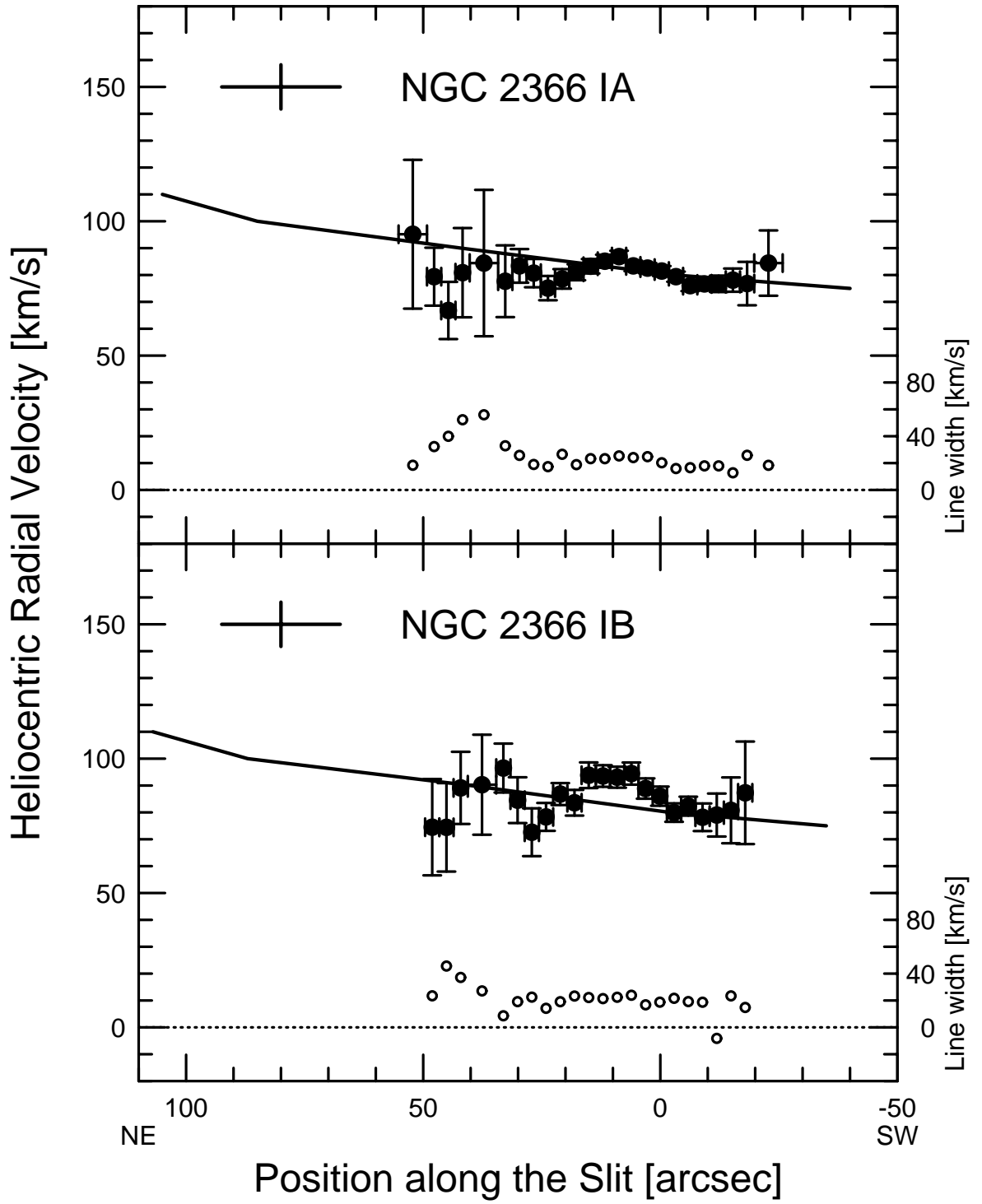


FIGURE 2 (b)

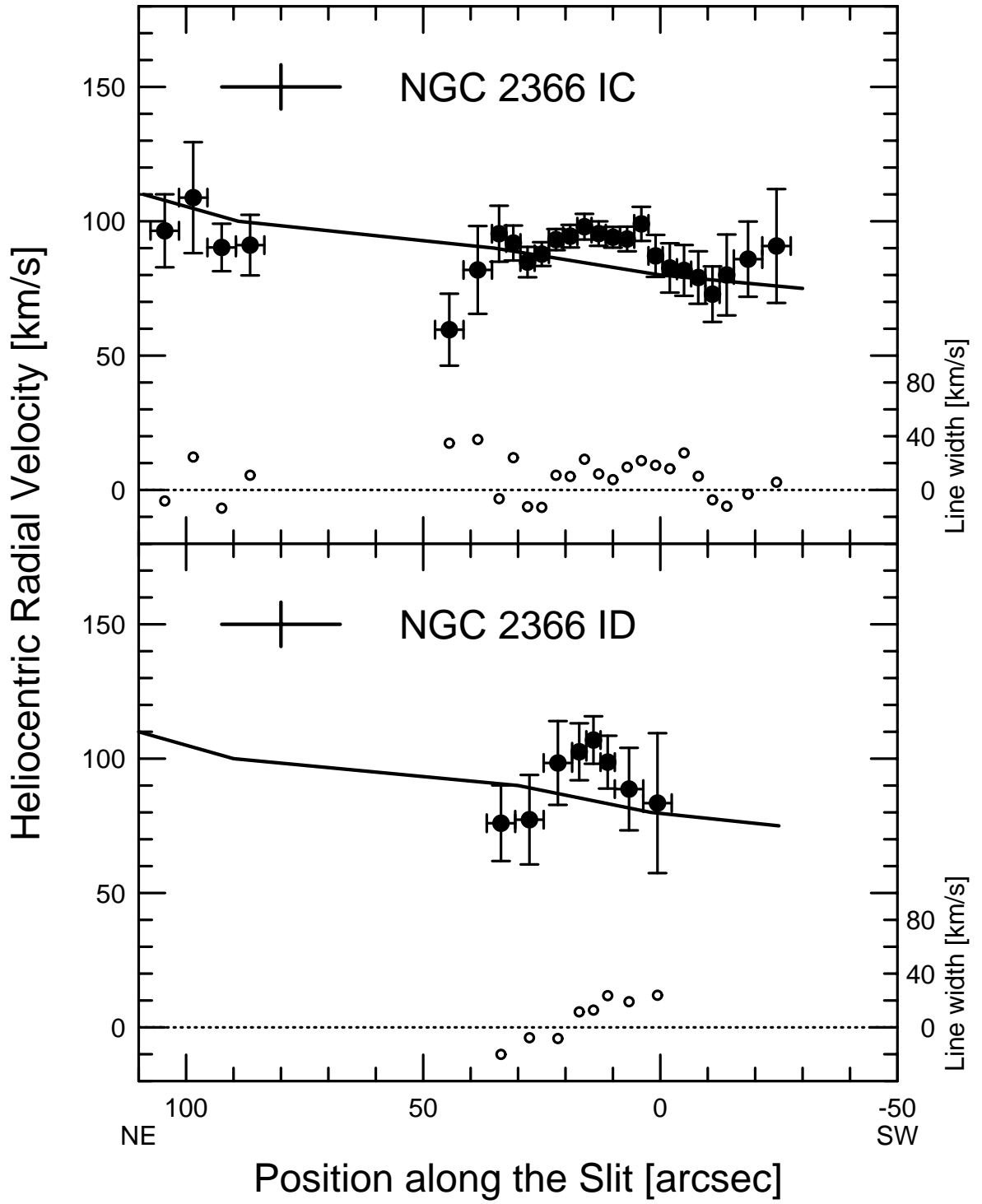


FIGURE 2 (c)

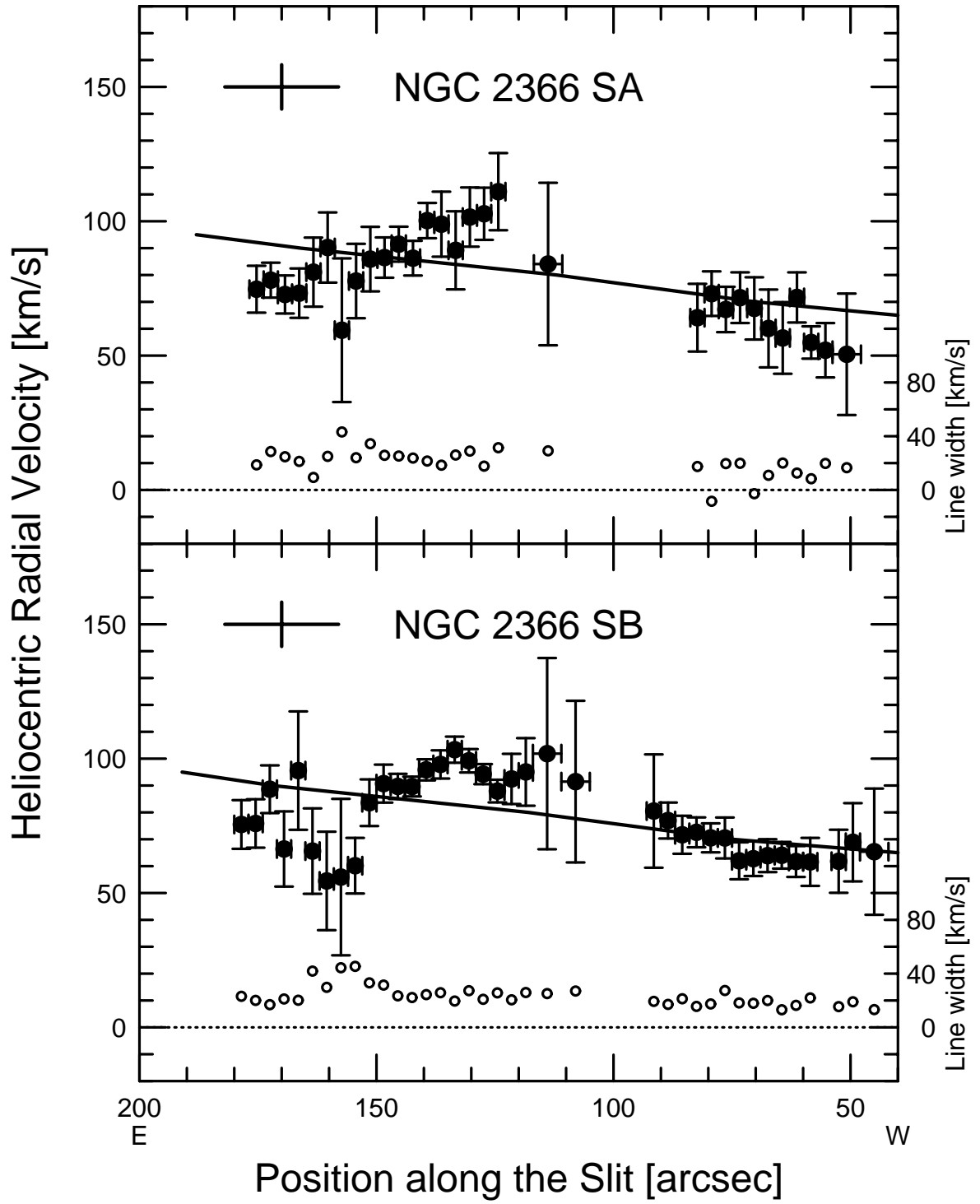


FIGURE 2 (d)

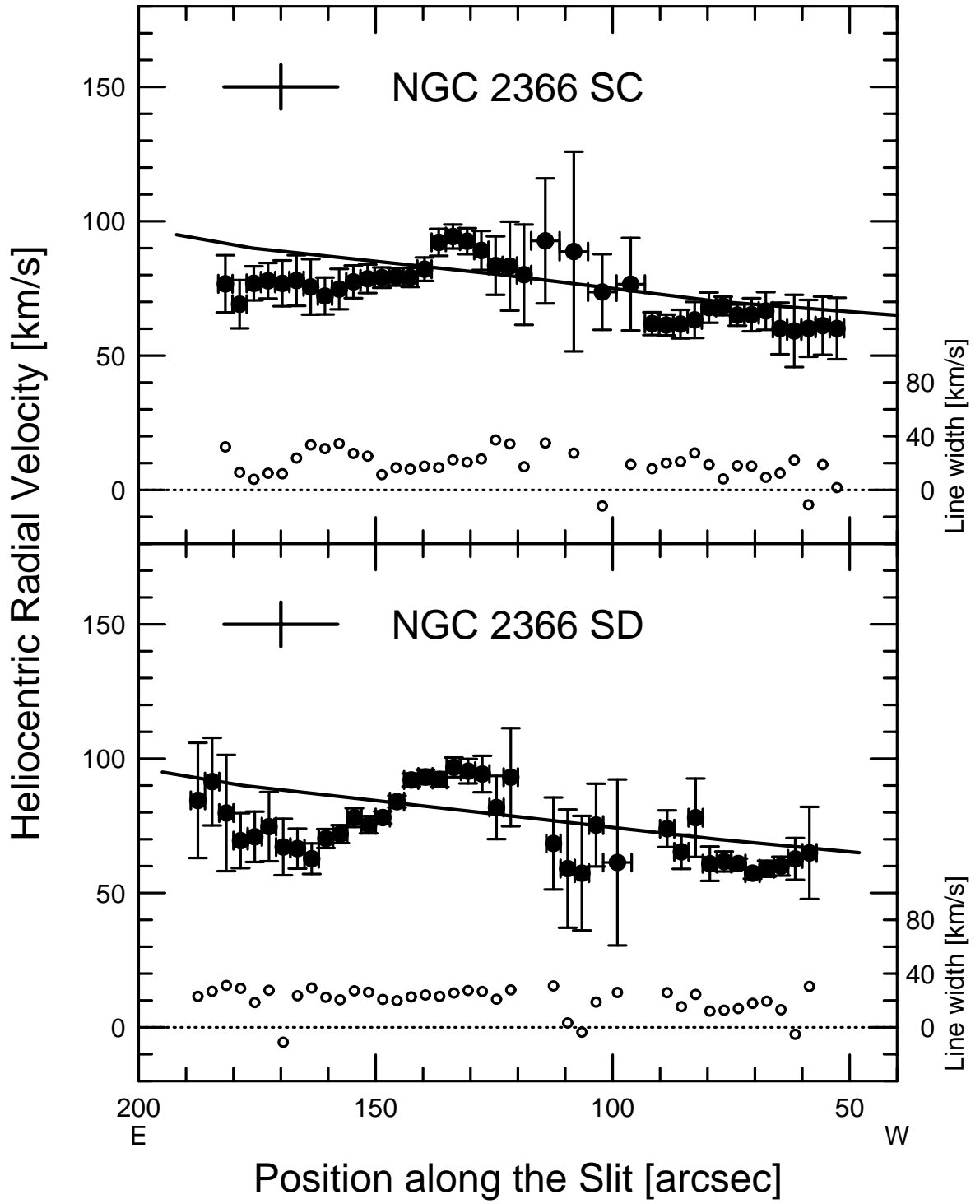




FIGURE 2 (e)

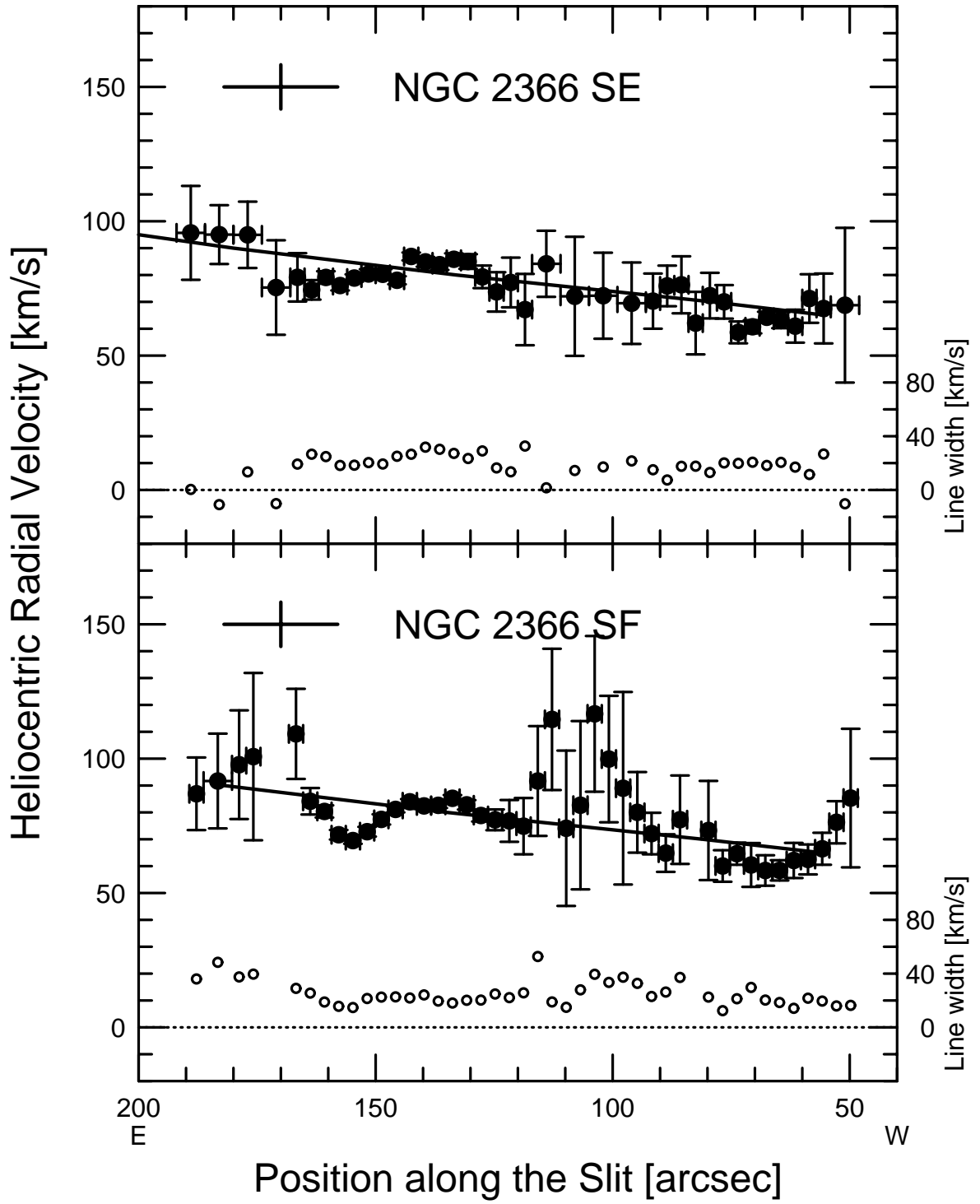


FIGURE 2 (f)

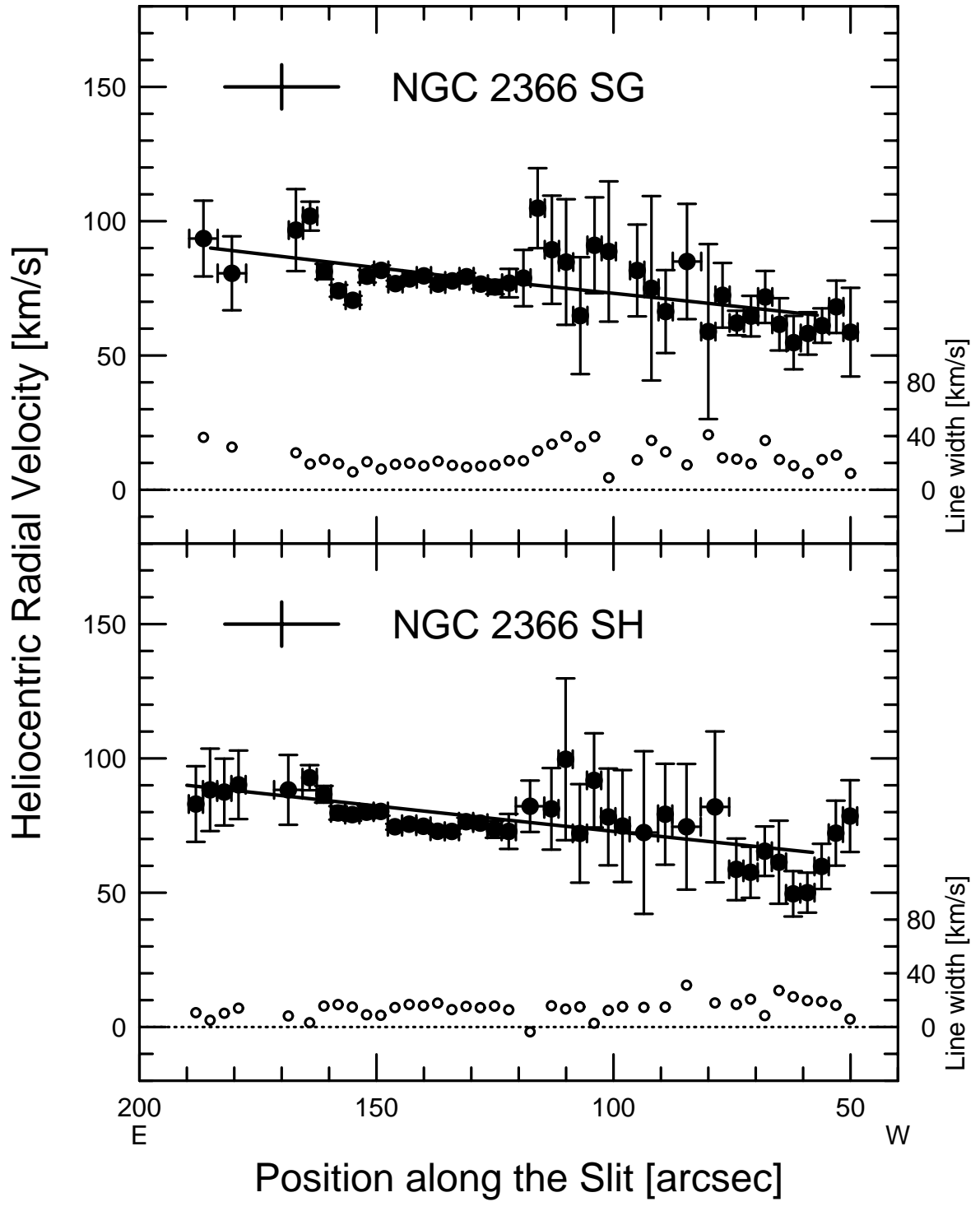


FIGURE 2 (g)

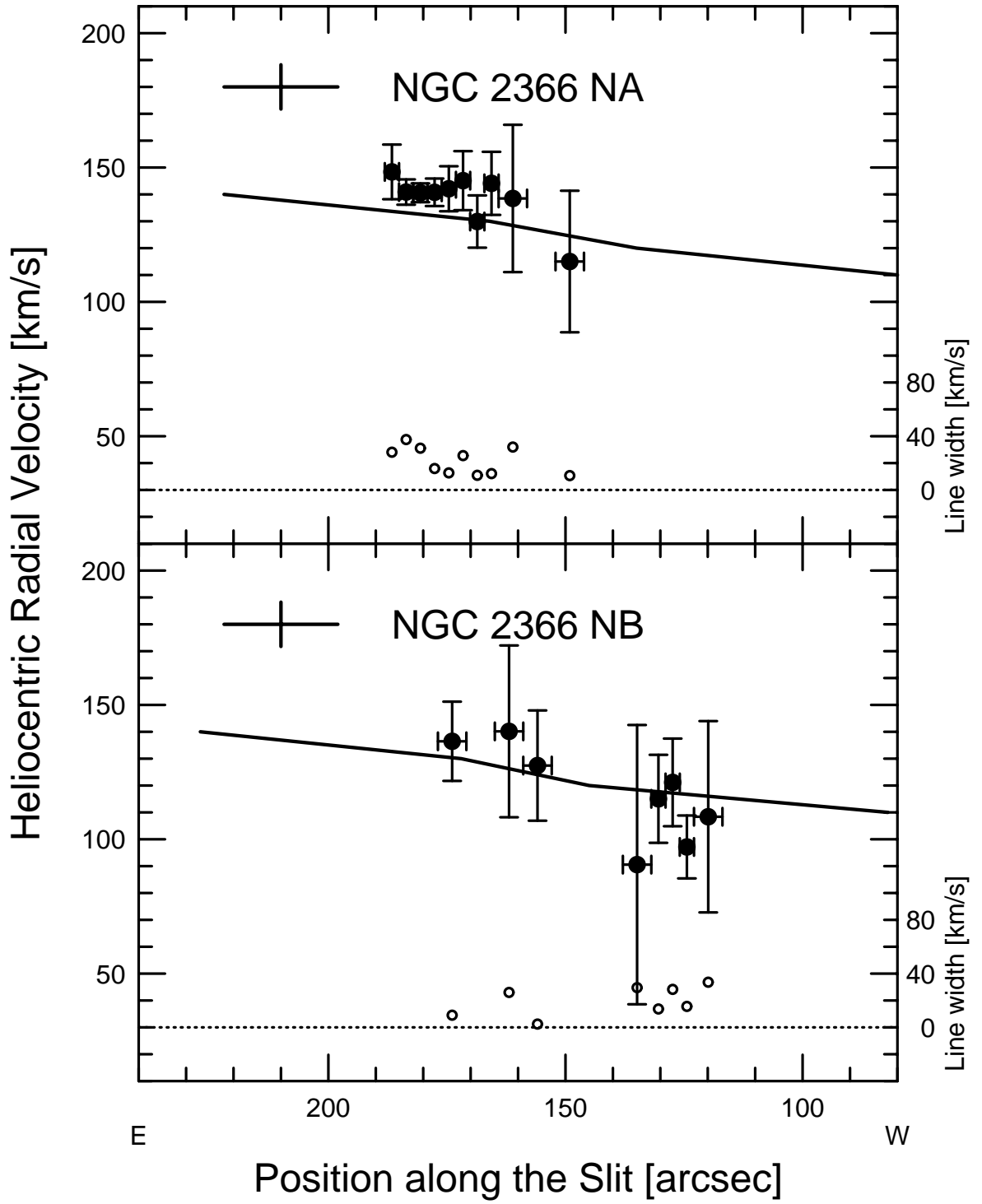


FIGURE 2 (h)

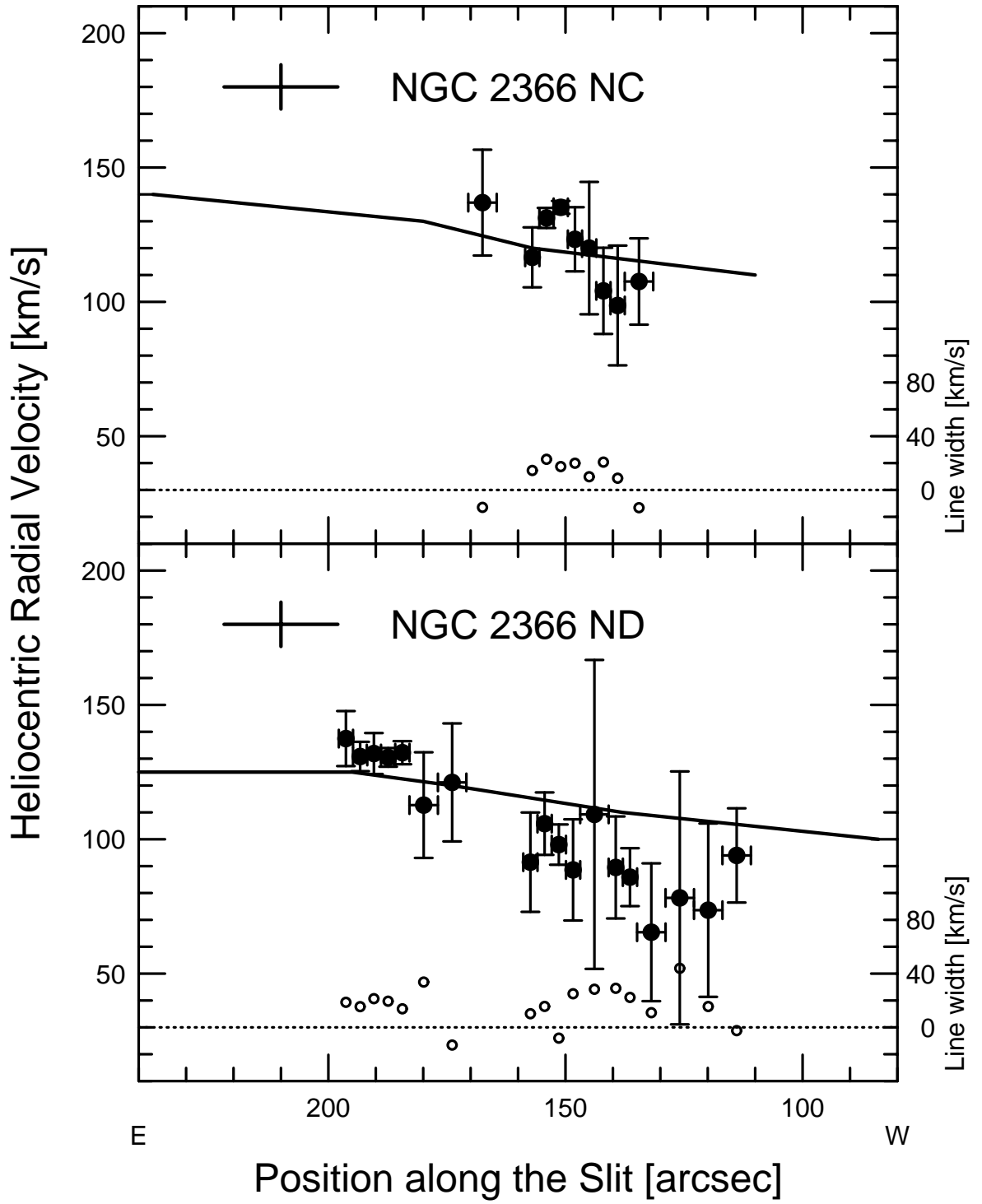


FIGURE 3 (a)

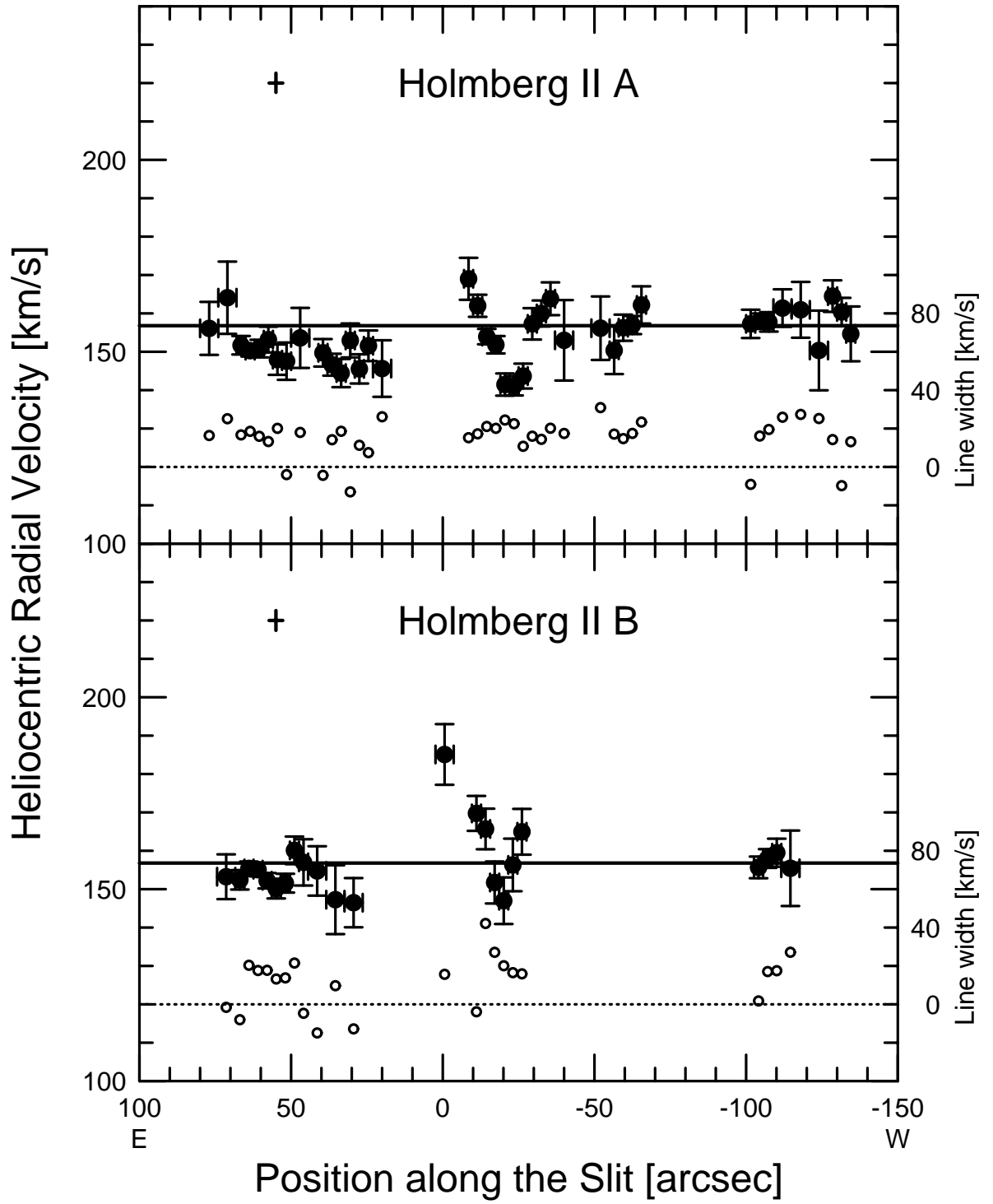


FIGURE 3 (b)

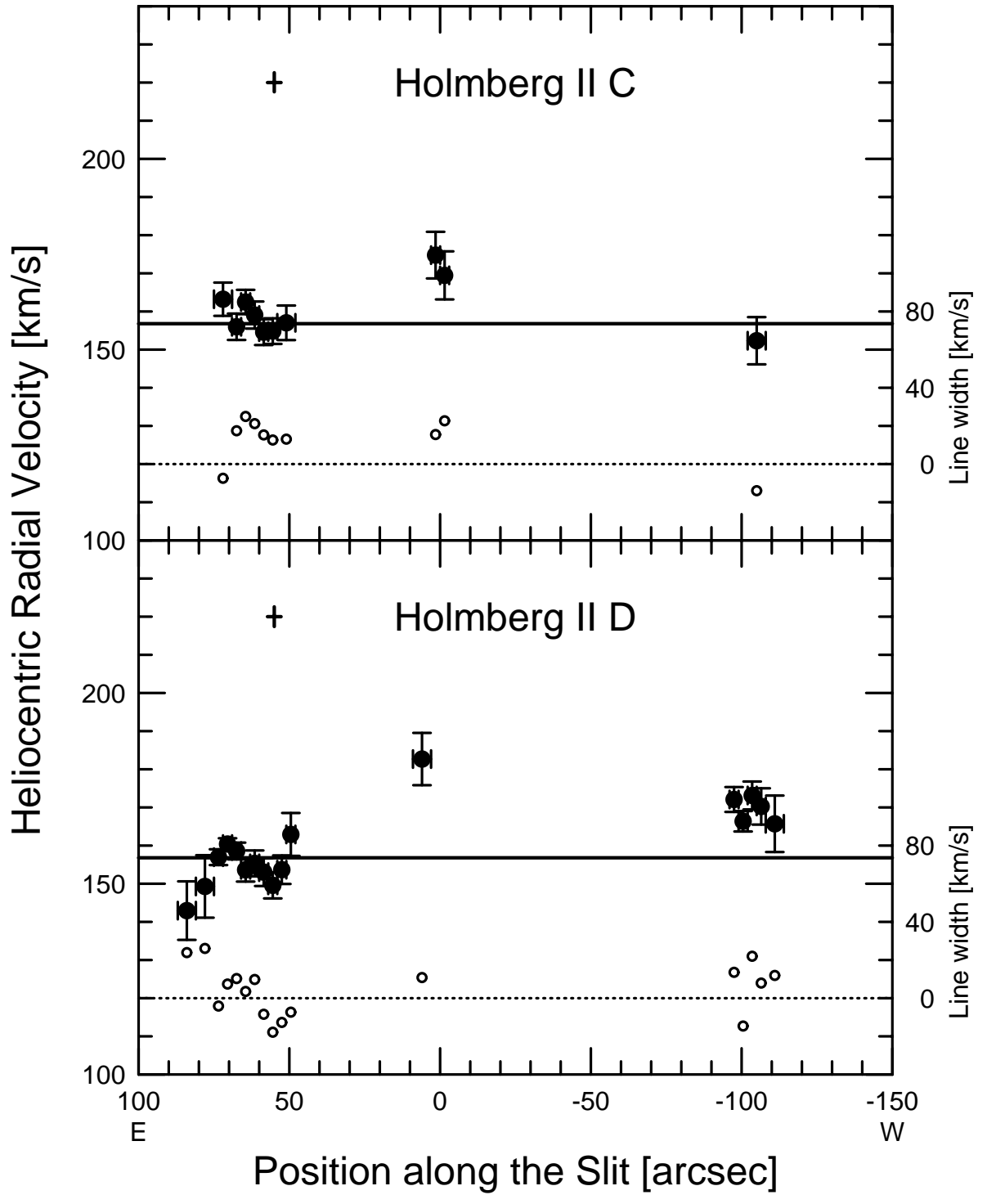


FIGURE 3 (c)

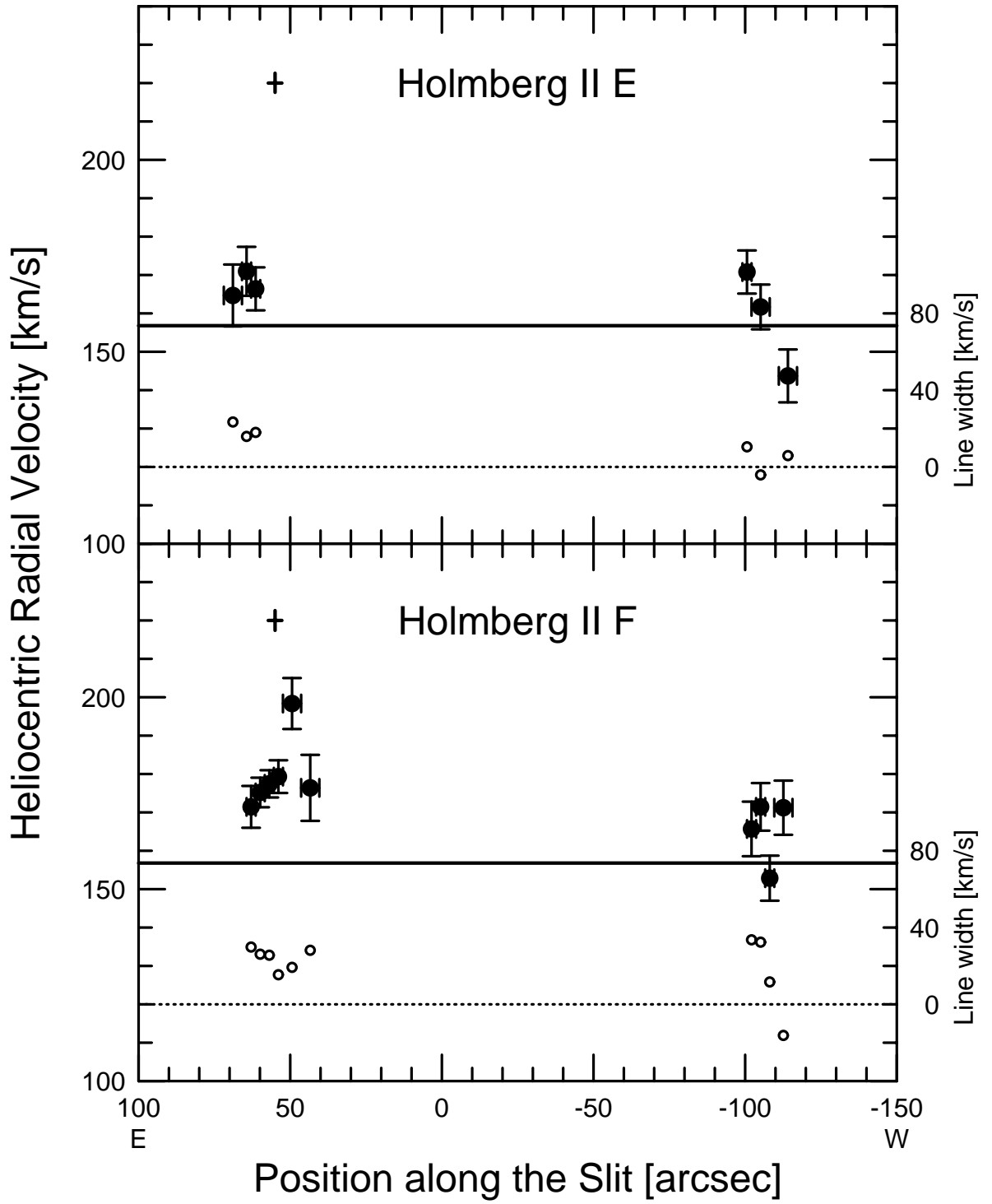


FIGURE 3 (d)

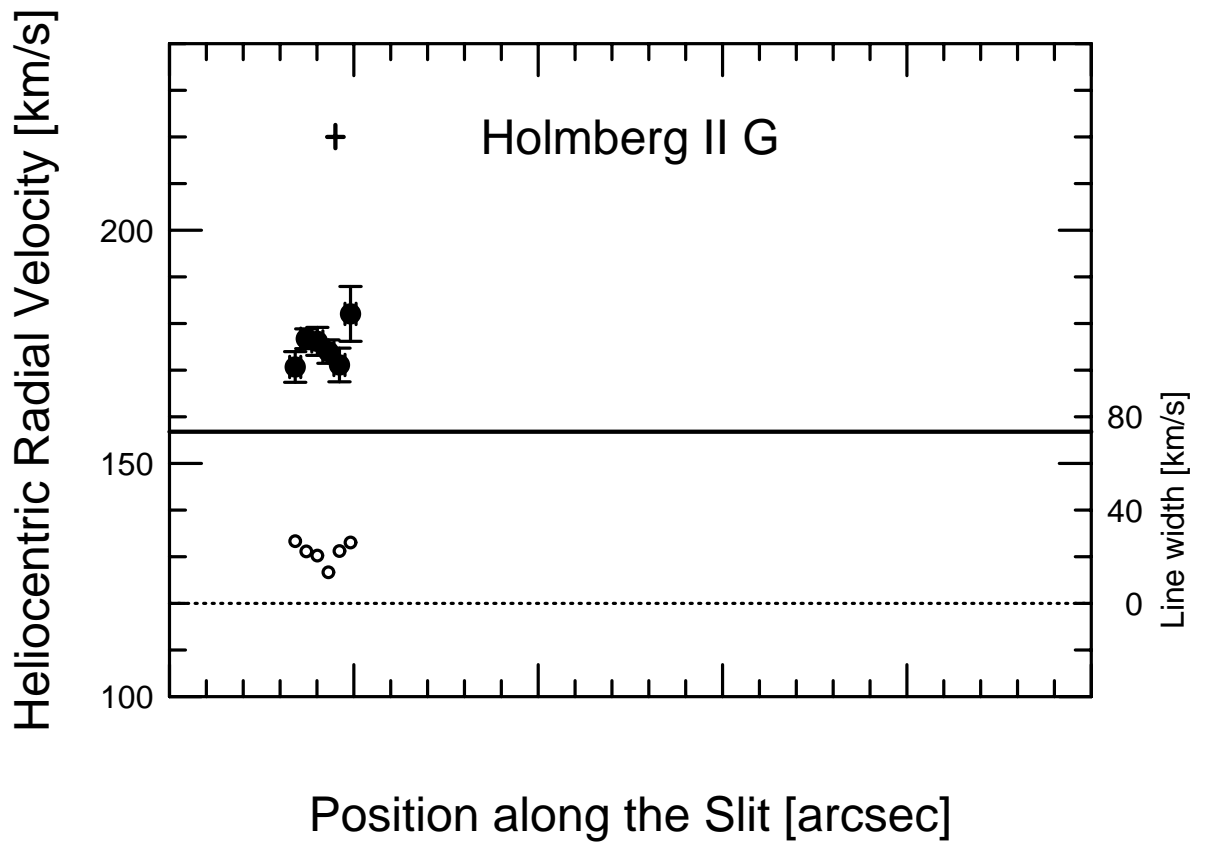




FIGURE 4 (a)

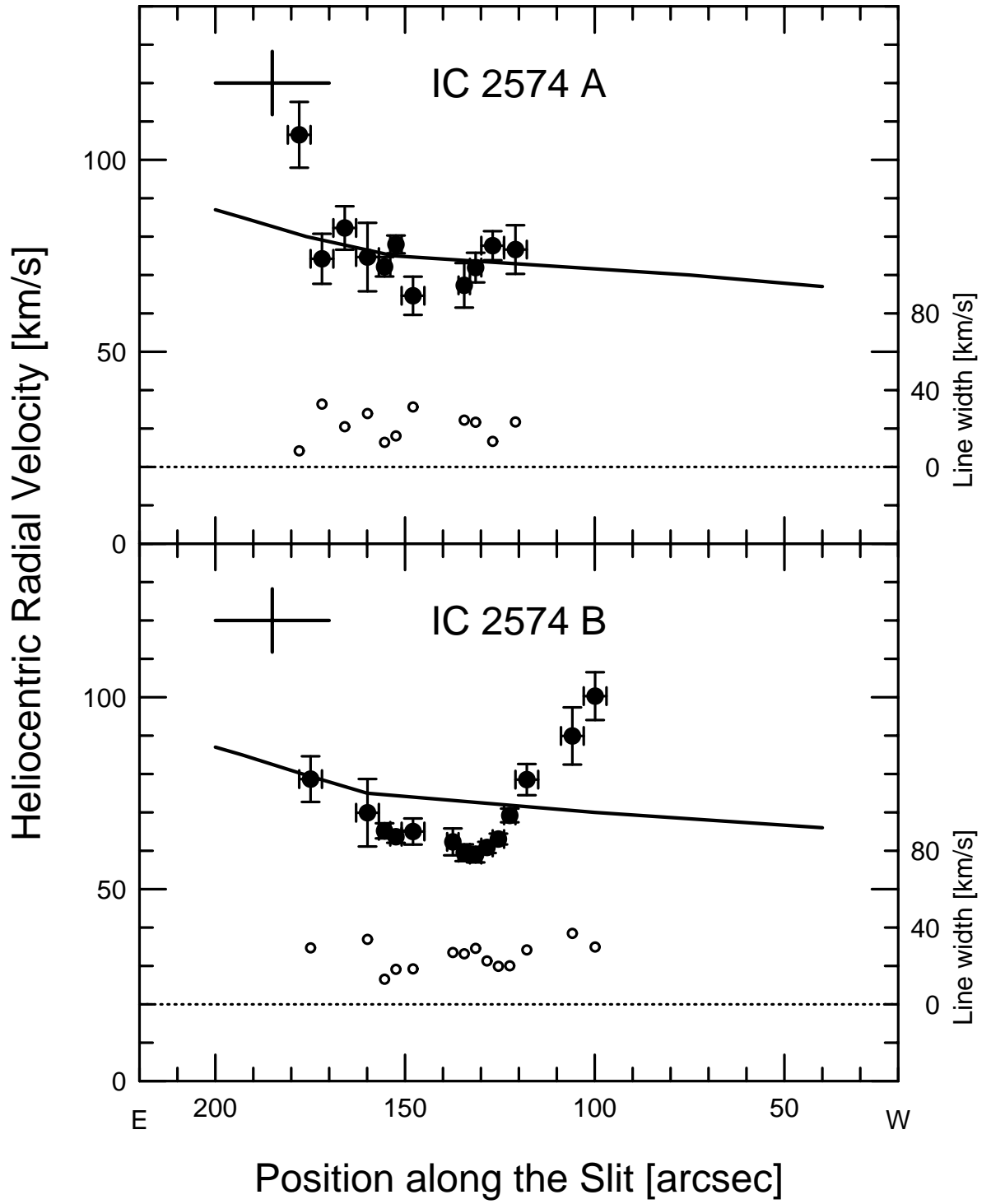


FIGURE 4 (b)

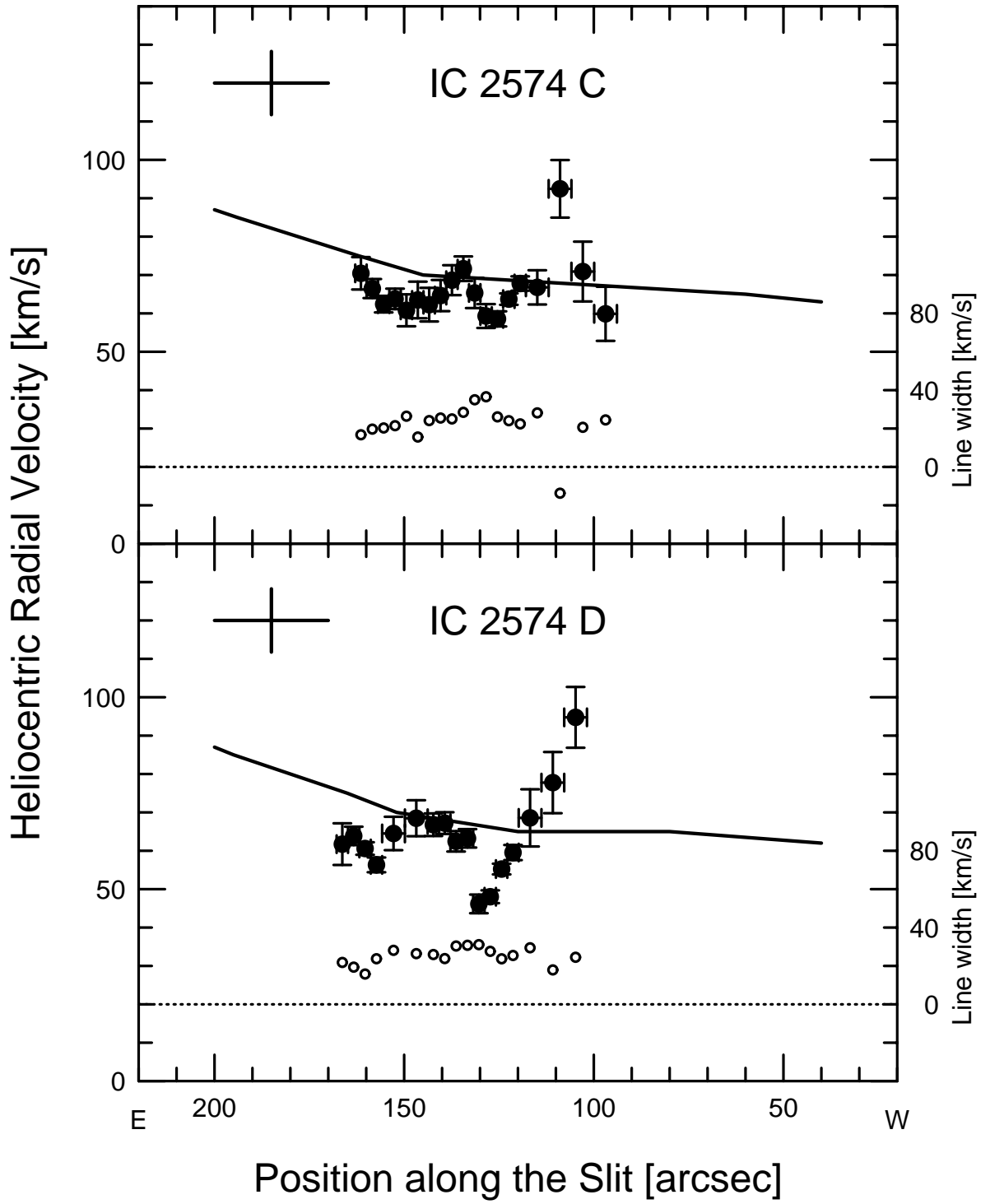


FIGURE 4 (c)

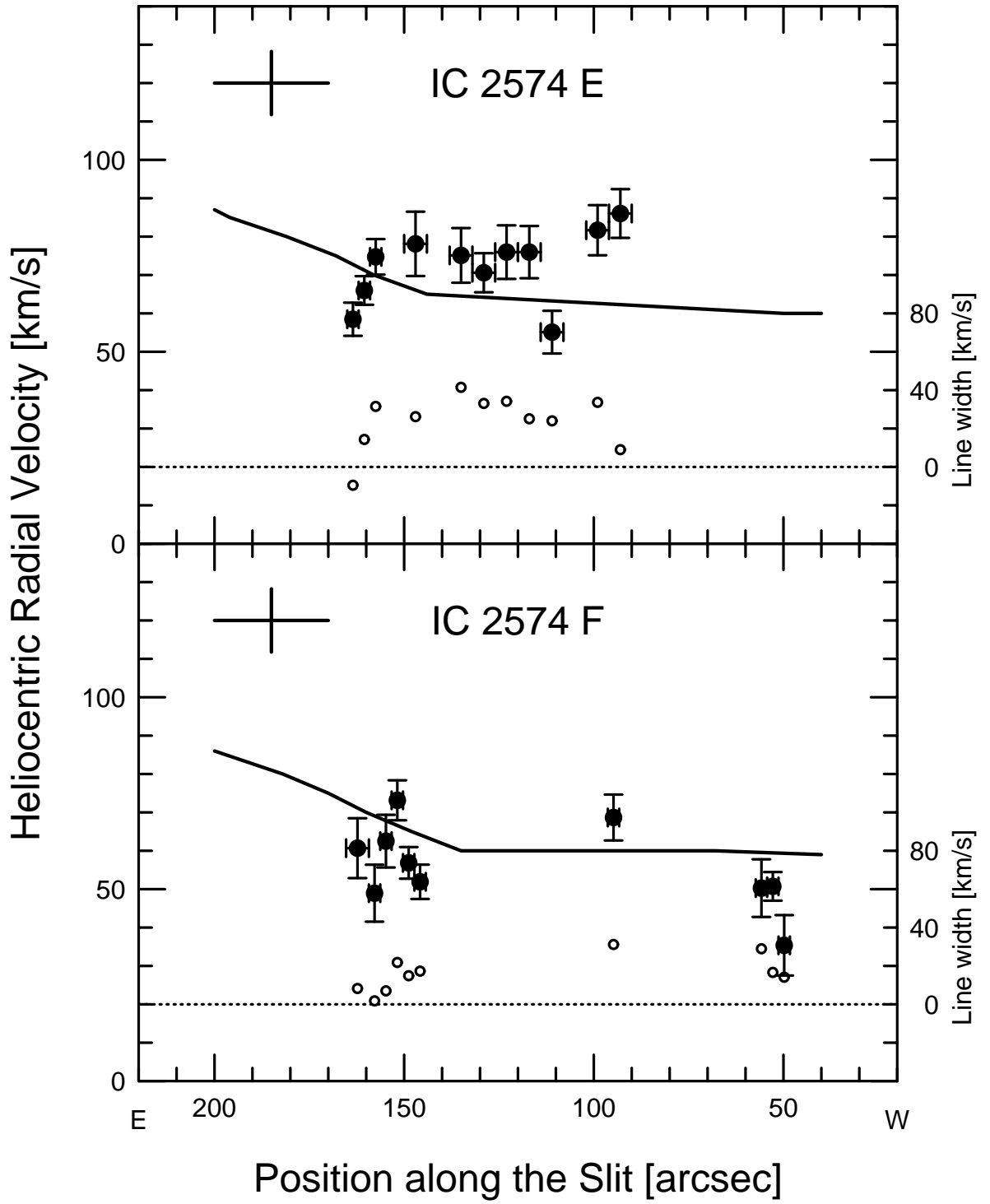


FIGURE 5 (a)

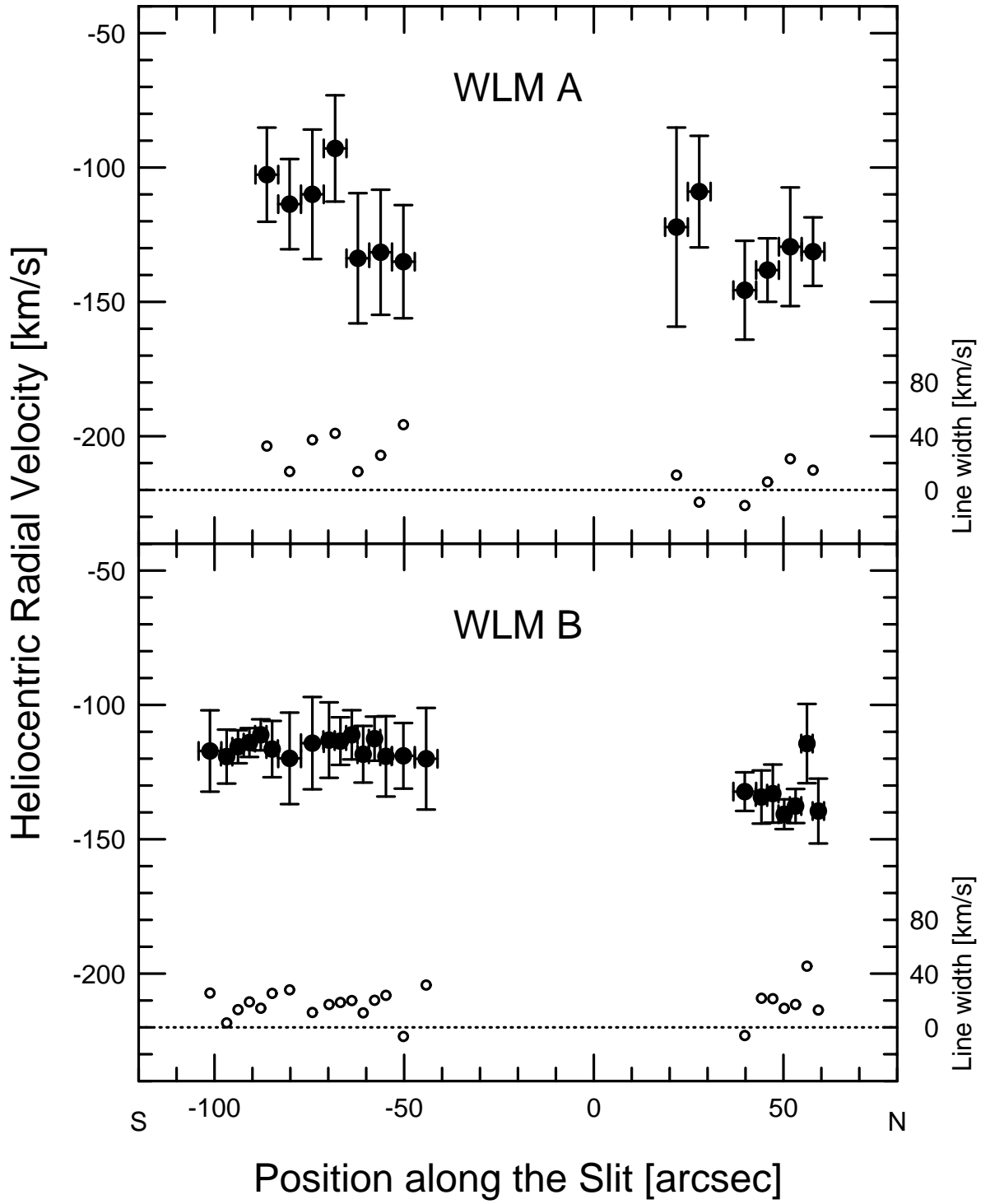


FIGURE 5 (b)

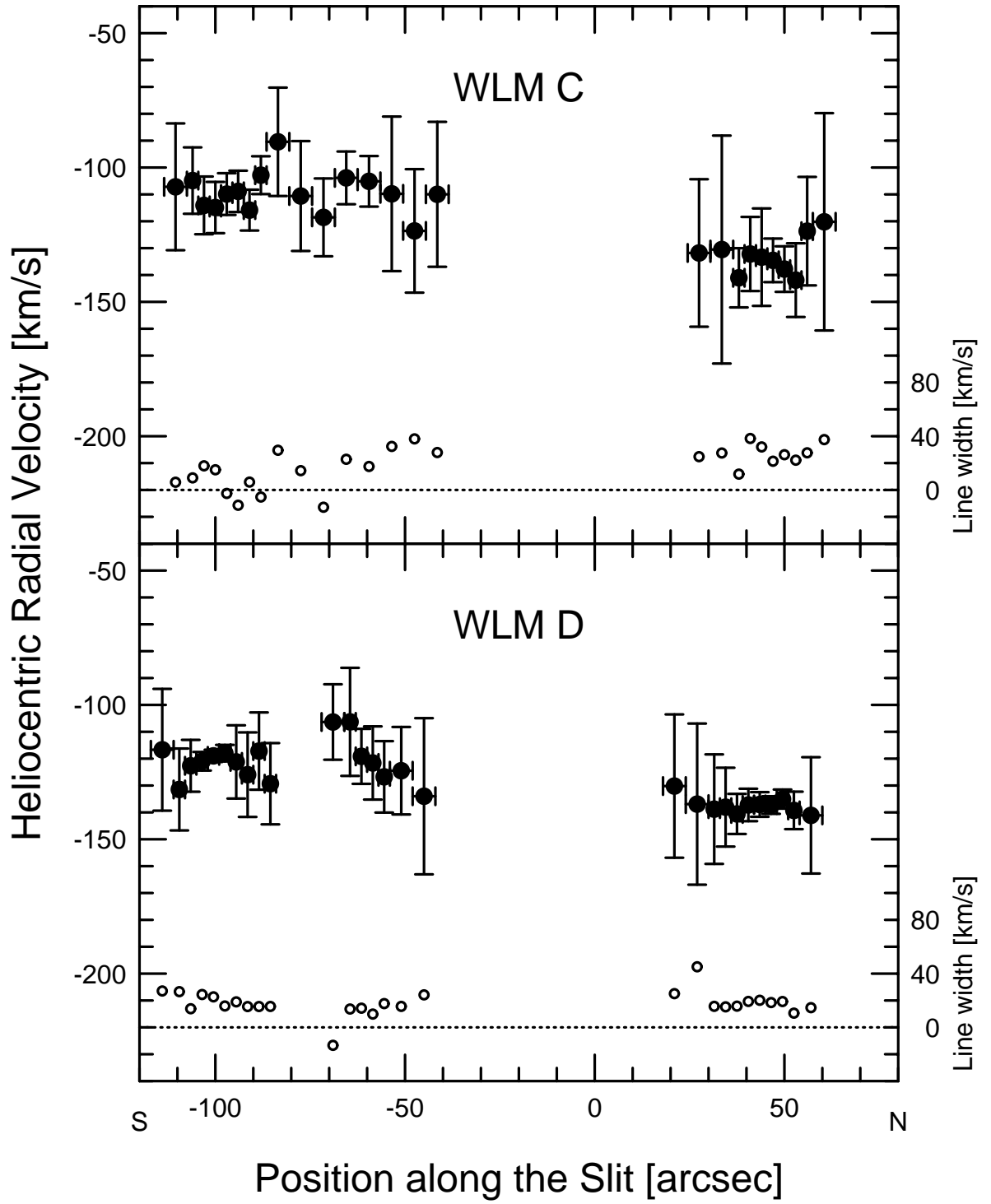


FIGURE 5 (c)

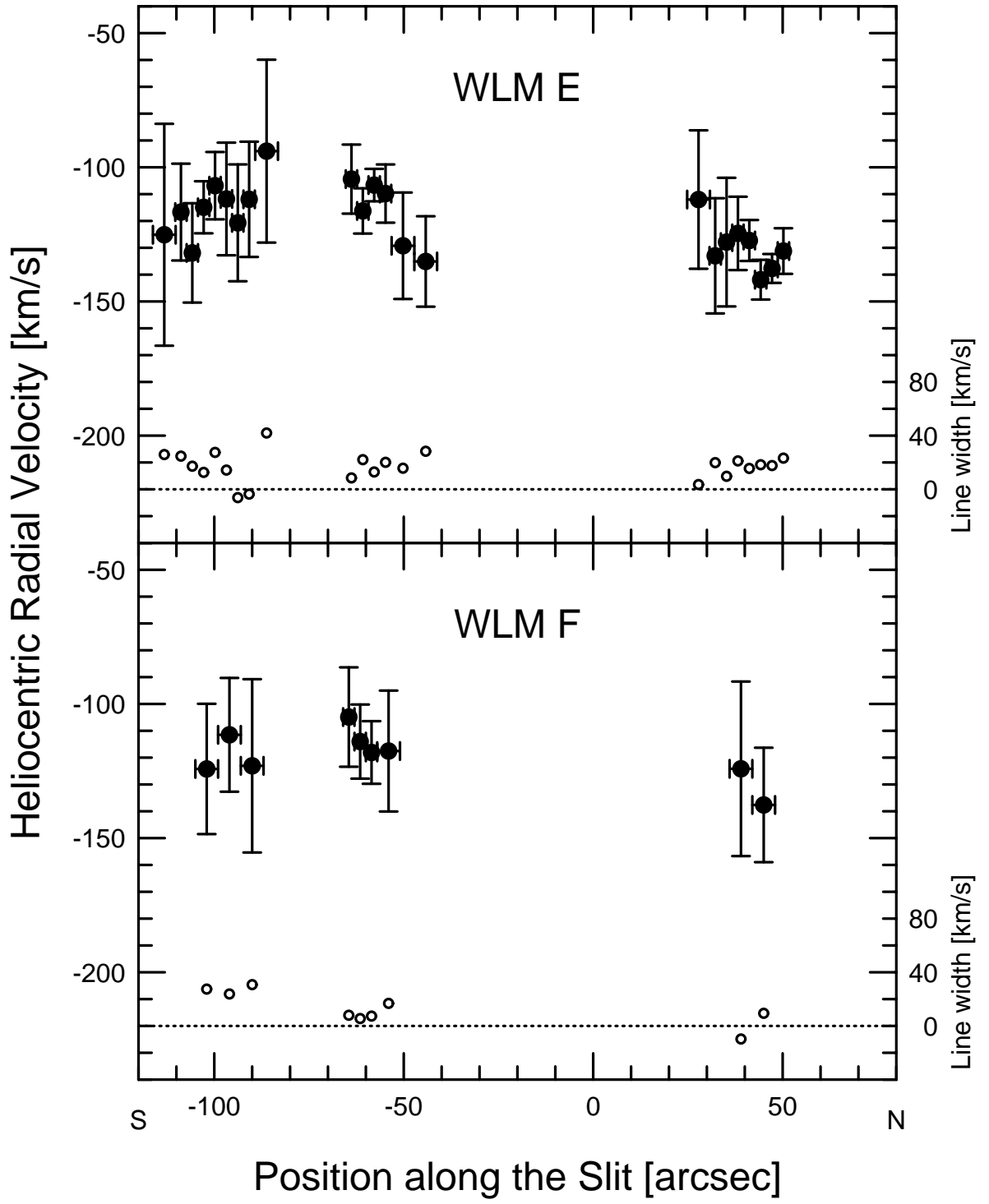


FIGURE 5 (d)

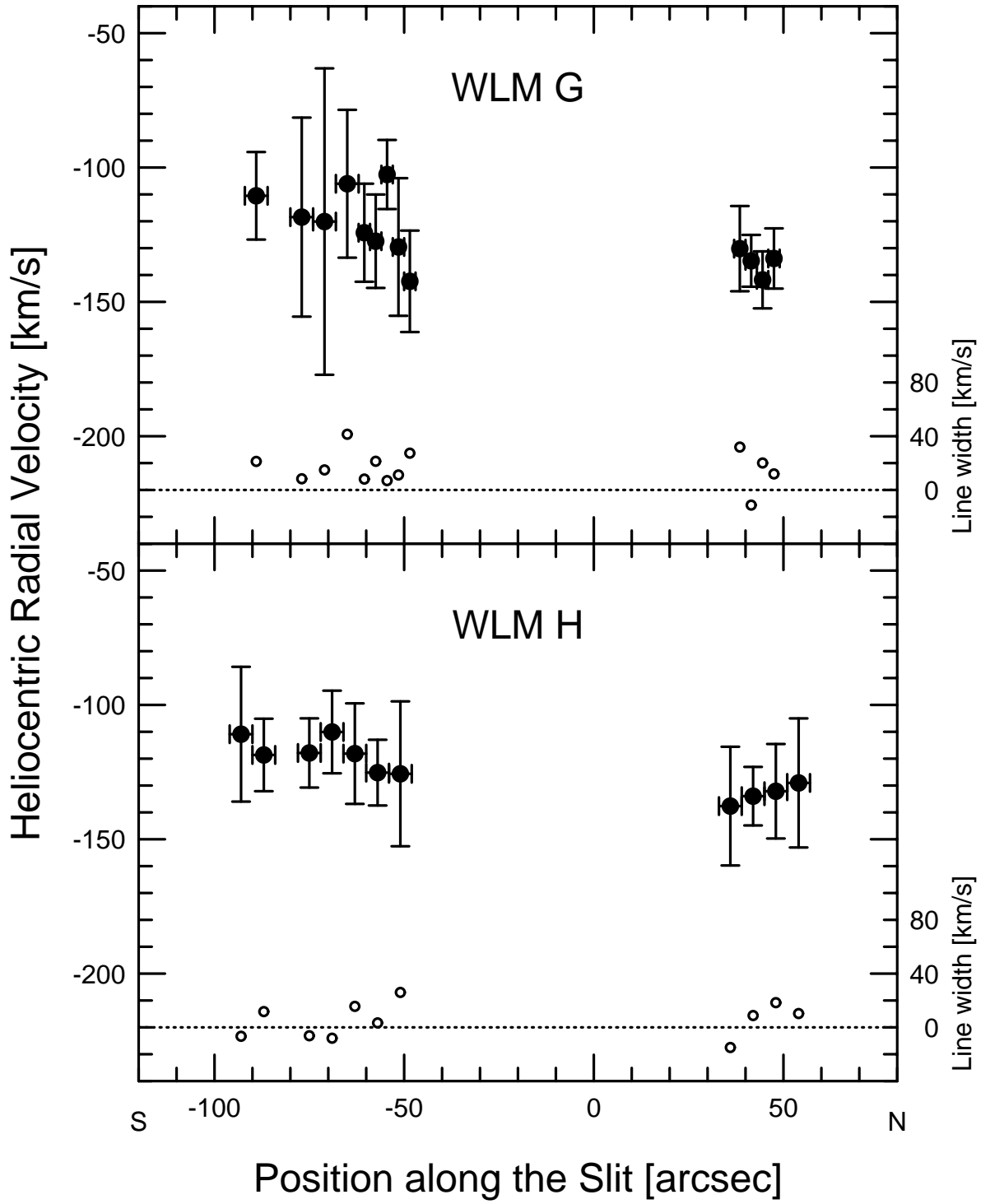


FIGURE 5 (e)

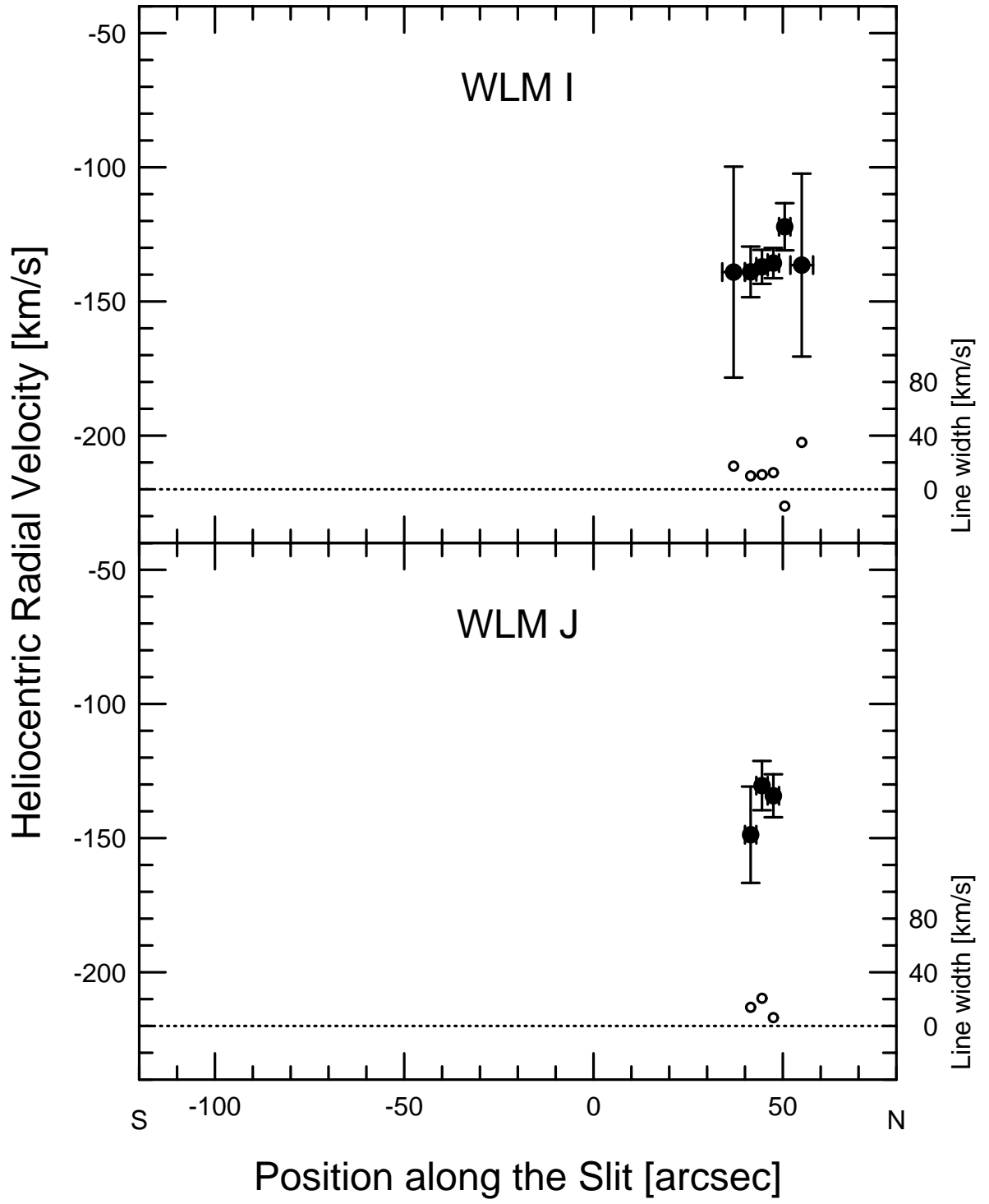




FIGURE 6

Classification of the P-V Diagram

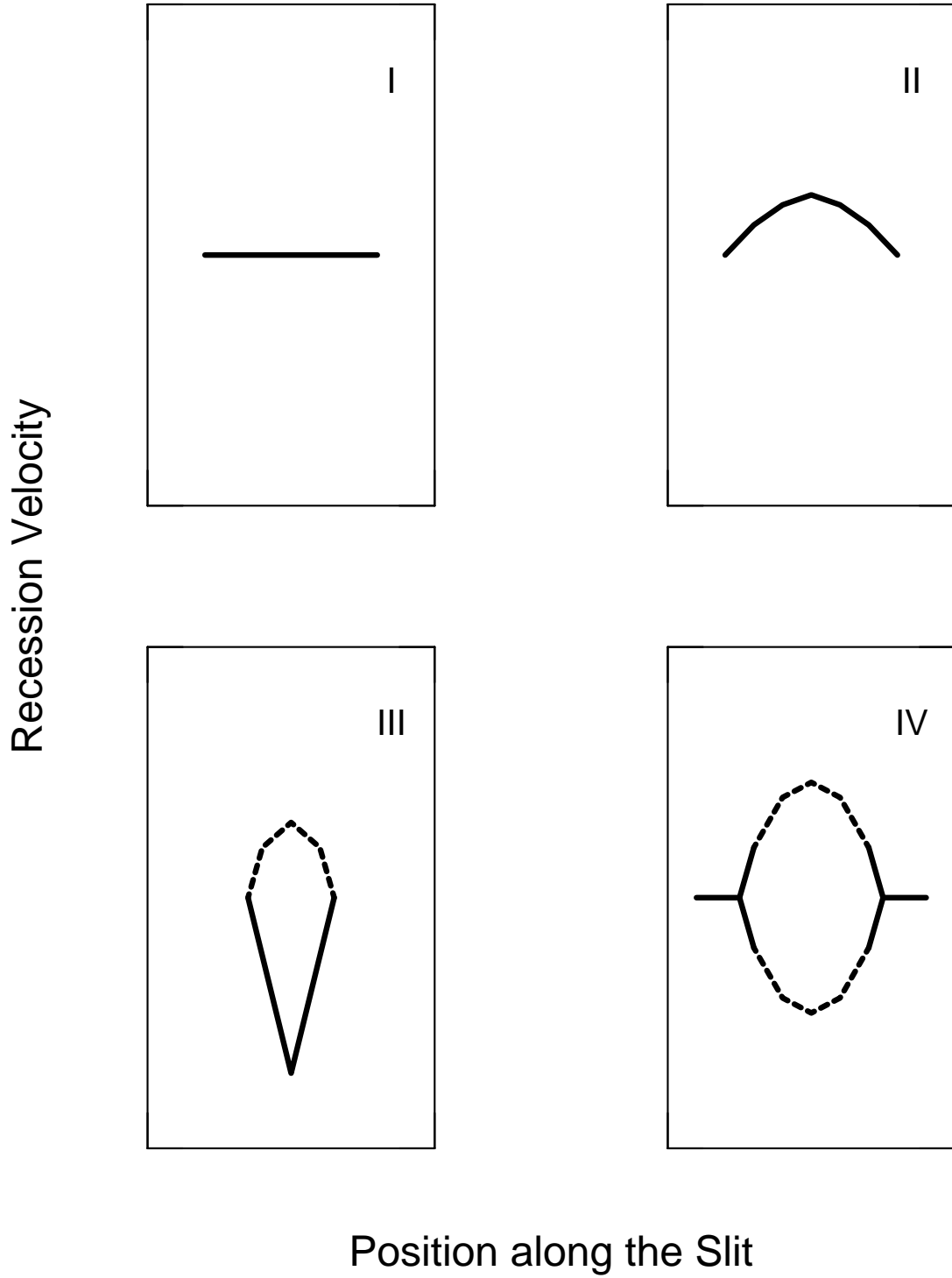
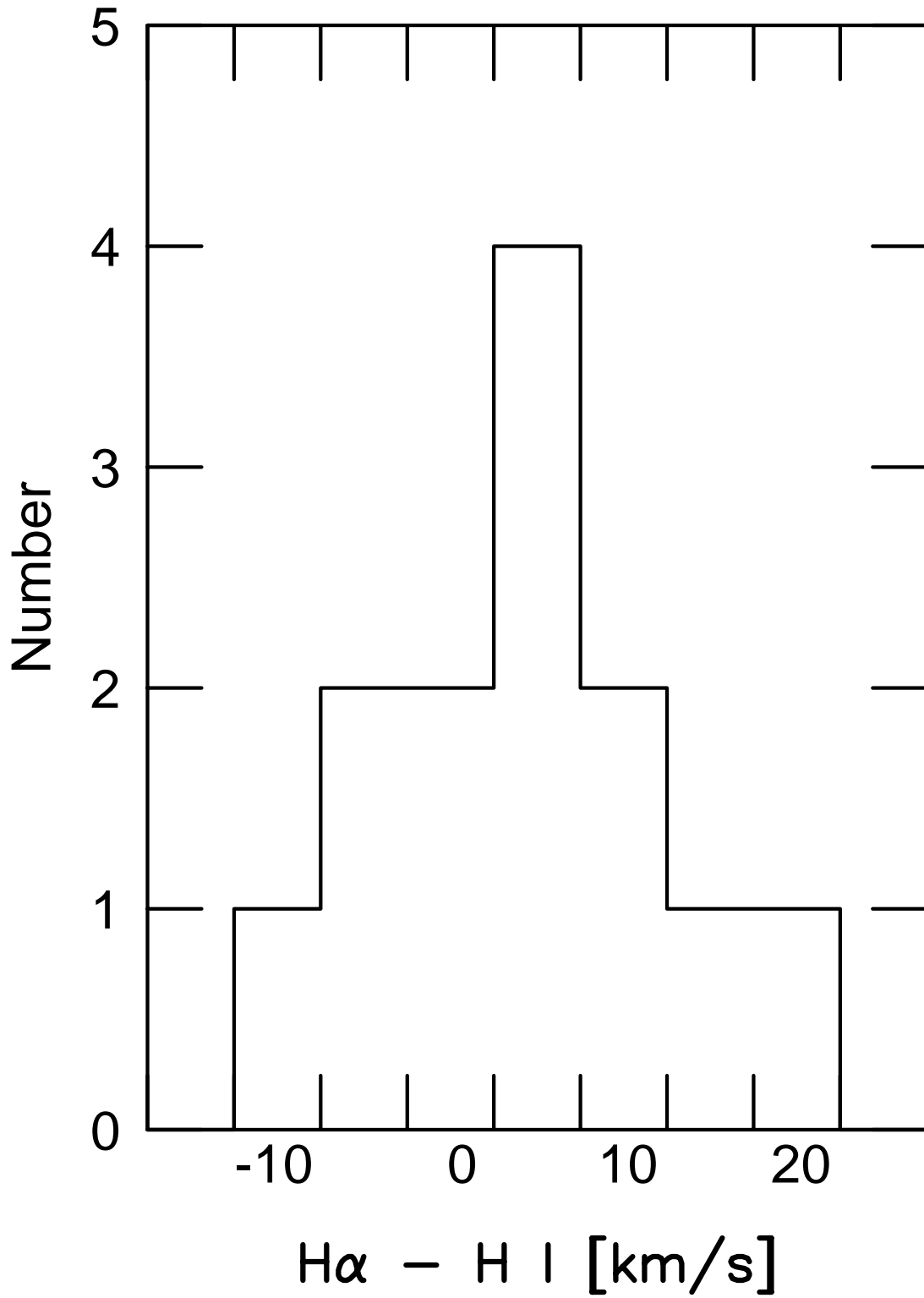


FIGURE 7

### Bulk Motion of the H II Regions



# H-Alpha Velocity Fields of H II Regions in Nearby Dwarf Irregular Galaxies <sup>1</sup>

Akihiko Tomita

Department of Earth and Astronomical Sciences, Faculty of Education,  
Wakayama University, 930 Sakae-Dani, Wakayama 640-8510, Japan

Electronic mail: atomita@center.wakayama-u.ac.jp

Kouji Ohta, Kouichiro Nakanishi, Tsutomu T. Takeuchi <sup>2</sup>, and Mamoru Saitō

Department of Astronomy, Faculty of Science, Kyoto University

Sakyo-ku, Kyoto 606-8502, Japan

Electronic mail: ohta, nakanisi, takeuchi, saitom@kusastro.kyoto-u.ac.jp

Received 1997 December 29; accepted 1998 March 16

To be appeared in The Astronomical Journal, 1998 July issue

---

<sup>1</sup> Based on observations made at Okayama Astrophysical Observatory (OAO). OAO is a branch of the National Astronomical Observatory of Japan, an inter-university research institute operated by the Ministry of Education, Science, and Culture, Japan.

<sup>2</sup> Research Fellow of the Japan Society for the Promotion of Science.

## ABSTRACT

We present H $\alpha$  velocity fields of thirteen giant H II regions in four nearby dwarf irregular galaxies, NGC 2366, Holmberg II, IC 2574, and WLM. We classify the velocity features as well as the morphologies of the H II regions. The H $\alpha$  velocity features are divided into three categories; three H II regions show chaotic feature with a typical scale of variation of a few 100 pc in size and a few 10 km s<sup>-1</sup> in velocity, one shows expanding-bubble feature, and the remaining nine have calm velocity fields. There is a correlation between the H $\alpha$  velocity feature and the morphology of H II regions. We measured bulk motion of the H II regions relative to the ambient H I velocity for the H II regions with calm velocity fields and found a typical velocity difference of about 5 km s<sup>-1</sup>. We discuss a model for origin of star-forming regions based on the presence of the velocity difference between H $\alpha$  and H I gas as well as the H I characteristics.

*Subject headings:* galaxies: dwarf — galaxies: irregular — galaxies: ISM — galaxies: individual (NGC 2366, Holmberg II, IC 2574, WLM)

## 1. Introduction

Since dwarf irregular galaxies are slow and nearly rigid rotators, they are suitable for studying kinematical and morphological properties of star-forming regions and interaction with surrounding interstellar medium (ISM). Some dwarf irregulars have many H I holes (e.g., Puche *et al.* 1992); relation between the H I holes and the star formation activity was discussed but it is not yet clear. Roy *et al.* (1992) claimed that an extremely high-velocity exploding component is commonly associated with H II regions in dwarf irregular galaxies, but nature of the high-velocity component has not been understood. Star formation activities of some dwarf irregular galaxies, even of isolated ones, are as high as those of spiral galaxies (Hunter & Gallagher 1986), though the dwarfs do not have spiral arms. Saitō *et al.* (1992) proposed a model that collision of H I clouds from an extended H I envelope with a dense H I disk could be a star formation trigger based on the observations of the H $\alpha$  velocity field in IC 10. Tomita *et al.* (1993, 1994) presented the H $\alpha$  velocity fields in other four dwarf irregular galaxies and showed results which are consistent with the model by Saitō *et al.* (1992). However, the number of samples is still small and it is necessary to obtain more data to examine this model.

In this paper we present H $\alpha$  velocity fields in H II regions of another four nearby dwarf irregular galaxies and study the connection between the H $\alpha$  velocity field and the characteristics of the H II regions. In Sec. 2, we describe the sample galaxies, observations, and data reduction. We show the resultant position-velocity diagrams of the H $\alpha$  emission in Sec. 3. Discussions are given in Sec. 4.

## 2. Observations

## 2.1. Sample

We observed four galaxies, NGC 2366, Holmberg II, IC 2574, and WLM (the Wolf-Lundmark-Melotte system). They were selected from nearby, within about 3 Mpc, well-studied dwarf irregular galaxies at the location observable at the Okayama Astrophysical Observatory in Japan. We also preferred a small apparent inclination of the galaxy in order to avoid overlapping the H II regions along the line of sight.

Table 1 lists basic characteristics of the four observed galaxies. The second column tabulates the distance. NGC 2366, Holmberg II, and IC 2574 are members of the M 81 group, and the distances are about 3 Mpc. WLM is a member of the Local Group, and the distance is about 1 Mpc. The third column tabulates physical size of diameter of the galaxy. Three galaxies in the M 81 group have diameters of about 8 to 12 kpc and WLM has a smallest diameter of about 3 kpc. The fourth column tabulates the apparent inclination, where  $90^\circ$  refers to edge-on. The sixth column tabulates far-infrared (FIR) luminosity, which is an indicator of the present star formation rate of the galaxy. The seventh column tabulates the  $B$ -band luminosity, which is a measure of the luminous mass of the galaxy. The eighth column tabulates the dynamical total mass of the galaxy inferred from the H I observations. The last column tabulates the H I mass.

We use the H I velocity field data in literature to compare with our H $\alpha$  velocity fields. The high-resolution synthetic H I observations were made for NGC 2366 by Wevers *et al.* (1986) and Braun (1995), for Holmberg II by Puche *et al.* (1992), and for IC 2574 by Martimbeau *et al.* (1994). For WLM there is no synthetic observation, therefore, we do not have the H I velocity field map with a high spatial resolution suitable for comparison with our H $\alpha$  data. We searched for the velocity data of CO molecular emission in literature, and found only one report for NGC 2366 by Hunter & Sage (1993) with no detection of the emission.

## 2.2. Observations and Reduction

A long-slit  $H\alpha$  spectroscopy was carried out in 1994 at the Okayama Astrophysical Observatory (OAO) in Japan using the 1.88-m reflector with the Spectronebulagraph (an automatic slit scanning system, see Kosugi *et al.* 1995). We observed giant H II regions in four galaxies; for NGC 2366 most part of the giant H II complexes at the southern part of the galaxy and some positions at the northern part of the galaxy, for Holmberg II about a half of the H II regions which concentrate at the central part of the galaxy, for IC 2574 about a half of the most prominent H II complexes at the northwestern part of the galaxy, and for WLM most of the H II regions. The observed slit positions are shown on the  $H\alpha$  map of Fig. 1 and the observed H II regions are summarized in Table 2. Detailed description about individual H II region is given in Sec. 3.2.

A spectrograph with a grating of 1200 grooves  $\text{mm}^{-1}$  blazed at 7500  $\text{\AA}$  and a Photometrics CCD with  $512 \times 512$  pixels (pixel size of  $20 \mu\text{m} \times 20 \mu\text{m}$ ) was equipped at the Cassegrain focus. The dispersion was  $0.7 \text{\AA} \text{ pixel}^{-1}$ , or  $30 \text{ km s}^{-1} \text{ pixel}^{-1}$  at the  $H\alpha$  line. The slit was  $5.0''$  long and  $1.8''$  wide and the instrumental broadening corresponded to about  $1.3 \text{\AA}$  in FWHM. The slit length was longer than the size of each  $H\alpha$  emitting region and by using the spectra of the sky we could make a sky subtraction well. A CCD pixel corresponds to  $0.75''$ . A typical seeing size was  $2''$  to  $3''$ . A log of the observations is listed in Table 3.

The data reduction and analysis were performed with the IRAF in the usual manner (IRAF is the software developed in National Optical Astronomy Observatories). We binned the spectra in four adjacent CCD pixels ( $3.0''$ ) along the slit length at all of positions, except for the positions where the spectra have low signal-to-noise ratios, where we binned in eight pixels ( $6.0''$ ). Since most of the observed  $H\alpha$  emission-line profiles are symmetric and nearly Gaussian, we fitted a single Gaussian to the observed line to measure the central

wavelength and FWHM of the line. The error in determining the line center is about  $3 \text{ km s}^{-1}$  (corresponding to one tenth of the pixel size) to  $20 \text{ km s}^{-1}$  depending on the signal-to-noise ratios. The error of the measured FWHM is similar to that of the measured central wavelength.

### 3. Results

#### 3.1. Position-Velocity Diagram

We present all of our results in the form of position-velocity diagrams in Figs. 2 – 5. The abscissa indicates the position along the slit, and the width of the abscissa corresponds to the line length given in Fig. 1. The origin on the slit position, shown as  $0''$  on the abscissa, is listed in Table 4. The ordinates of diagrams in Fig. 2 indicate the heliocentric radial velocity of line center and the FWHM of line. The scale for the the central velocity is shown on the left-side ordinate and that for the FWHM is shown on the right-side ordinate. The filled circles indicate the central velocities of line profiles and the open circles indicate the FWHM of the lines. The horizontal error bar on a filled circle represents the binning size and the vertical error bar indicates an error in the measurement of the central velocity of a line. Within each panel, relative  $\text{H}\alpha$  intensities are propotional to the signal-to-noise ratios and these are almost inversely propotional to sizes of the vertical error bars. We corrected the instrumental broadening to obtain the FWHM. The FWHMs shown are, thus, due to the thermal broadening which is estimated to be about  $10 \text{ km s}^{-1}$  corresponding to  $10^4 \text{ K}$  and the motion of the ionized gas integrated in the line of sight. The dotted line in each diagram shows the  $0 \text{ km s}^{-1}$ -level of the FWHM; the correction for the instrumental broadening could make negative values of FWHM for some lines with low signal-to-noise ratios. The thick curve indicates the H I velocity taken from literature. The cross in the upper-left corner of the panel shows the accuracy of the H I observations. The full length



of the horizontal line of the cross indicates the FWHM of the beam for the H I isovelocity map. The half length of the vertical line of the cross indicates the channel spacing of the H I observations.

### 3.2. Results of Individual Galaxies

#### 3.2.1. NGC 2366

The resultant sixteen position-velocity diagrams are shown in Fig. 2, where the length of abscissa corresponds to  $160''$  or 2.7 kpc at NGC 2366. The H II regions are concentrated at the southern part of the galaxy, and the most prominent H II complex has another name of NGC 2363. There is the second prominent H II complex at the east of NGC 2363; following Arsenault & Roy (1986) we call this H II region NGC 2366-III.

In NGC 2363 the  $H\alpha$  velocity field is calm at the central regions where the intensities of the  $H\alpha$  emission are most powerful; in the diagrams the central regions are located on  $20''$  to  $-10''$  at the slit position IA,  $150''$  to  $130''$  at the slit positions SE, SF, SG, and SH. The  $H\alpha$  velocity is almost the same as the H I velocity, and the line width is almost constant at  $20 \text{ km s}^{-1}$ . The FWHM of about  $20 \text{ km s}^{-1}$  and the calm velocity field at the central regions of NGC 2363 are consistent with the measurement by Arsenault & Roy (1986) who obtained the velocity dispersion of the integrated  $H\alpha$  profile of NGC 2363 (denoted as NGC 2366 I in their paper) to be  $23 \text{ km s}^{-1}$ . Terlevich & Melnick (1981) showed that NGC 2363 is on the size-velocity dispersion relation of the extragalactic H II regions which is expected for self-gravitating systems.

Unlike at the central regions, the  $H\alpha$  velocity field is curved at the outer regions in NGC 2363; see the slit positions IC, ID, SA, SB, SC, and SD. The typical scale of the variation of velocity is  $20''$  to  $30''$  corresponding to about 200 pc in size, and  $10$  to  $30 \text{ km s}^{-1}$

in velocity. An expanding shell-like velocity feature is seen at the position of  $180''$  to  $150''$  on the slit SB, east side of NGC 2363. By comparing with the  $H\alpha$  image of Fig. 1 (a), location of the shell-like velocity feature corresponds to  $H\alpha$  filaments.

The slit positions of IA to ID were located crossing the northwestern part of NGC 2363. From the center to outer region of NGC 2363 (from IA to ID), the  $H\alpha$  velocity rises from  $85$  to  $110 \text{ km s}^{-1}$ , drifting away from the H I velocity. The line width is almost constant at  $20 \text{ km s}^{-1}$  except for the regions with poor signal-to-noise ratios. The rise of the  $H\alpha$  velocity is also shown in diagrams of the slit positions SA to SC as an upturn velocity gradient at around  $150''$  to  $130''$ . The variation of the position-velocity diagrams is consistent with the [O III] velocity field given by Roy *et al.* (1991)'s Fig. 7, in which a high velocity ridge with an altitude of about  $10 \text{ km s}^{-1}$  appears in the northwest direction from the core of NGC 2363.

The  $H\alpha$  velocity of the second prominent H II region, NGC 2366-III, is shown at around the position of  $90''$  to  $50''$  on the slits SA to SH. The velocity field is calm in general, though the  $H\alpha$  velocity is curved at the slit positions SF to SH. The  $H\alpha$  velocities at the intense  $H\alpha$  regions are blue-shifted by several to  $10 \text{ km s}^{-1}$  than the H I velocity.

The H II regions at the northern part of the galaxy are one to two orders of magnitude less intense in the  $H\alpha$  light compared with the southern two prominent ones. The  $H\alpha$  velocity field shown on the slit positions NA to ND is not so curved and nearly the same as the H I velocity, though the signal-to-noise ratio is poor. Only two regions, at the position of  $170''$  to  $190''$  on the slit NA and at the position of  $180''$  to  $200''$  on the slit ND, have sufficient signal-to-noise ratios. Each of these two regions corresponds to small circular H II regions (see Fig. 1(a)); hereafter we call them the H II region NGC 2366 NA and ND, respectively; see Fig. 1 (a) and Table 2.

### 3.2.2. High-Velocity Expanding Component in NGC 2363

Roy *et al.* (1991) showed that at the central region of NGC 2363 the profiles of the emission lines split corresponding to an expanding velocity of  $45 \text{ km s}^{-1}$ , and that whole NGC 2363 has a high-velocity expanding component with a velocity width of about  $1000 \text{ km s}^{-1}$ . Roy *et al.* (1992) and González-Delgado *et al.* (1994) reported confirmations of the high-velocity expanding component, and Roy *et al.* (1992) claimed that any models could not explain the large expanding velocity. Hunter *et al.* (1993) presented a deep  $\text{H}\alpha$  imaging and found many  $\text{H}\alpha$  filaments around NGC 2363, though the connection with the high-velocity expanding component is unknown.

In the present observations, we could detect neither the broad line component with a few times  $1000 \text{ km s}^{-1}$  nor the splitting profile with the expanding velocity of  $45 \text{ km s}^{-1}$  at the central region of NGC 2363. Both of Roy *et al.* (1992) and González-Delgado *et al.* (1994) extracted the high-velocity expanding component by picking up the residuals after fitting the emission-line profile with a single Gaussian and the peak intensity of the broad component is only 1% of that of the observed original line. We should note that the observed line profile deviates from the complete Gaussian in general and that the shape of the wing of the profile depends on the conditions of the spectrograph; in our data we could not confirm the existence of the broad line component with more than  $1000 \text{ km s}^{-1}$ . The expanding bubble with the velocity of  $45 \text{ km s}^{-1}$  was clearly shown by Roy *et al.* (1991) in [O III] emission line. The region where the [O III] line splits has an area of about  $5'' \times 5''$  as shown in Fig. 5 of Roy *et al.* (1991). In our spectroscopy, one data points in Fig. 2 sampled an area of  $1.''8 \times 3.''0$  and the spacing of slit scan was  $6.''0$ . Because of the sparse spatial sampling in our scanning, we may miss the regions showing the line splitting.

### 3.2.3. *Holmberg II*

The resultant seven position-velocity diagrams are shown in Fig. 3. The width of the abscissa corresponds to  $250''$  or 3.9 kpc at Holmberg II. The observed H II regions are divided into three blocks; eastern, central, and western blocks. The eastern block consists of northern (slit positions A to D) and southern (F and G) parts and the western block consists of northern (A and B) and southern (D to F) parts as shown in the  $H\alpha$  map of Fig. 1(b). Hereafter we call these five regions Holmberg II NE, SE, Center, NW, and SW; see Fig. 1 (b) and Table 2.

The Center has a steep V-shaped velocity feature as shown in the diagrams for the slit positions A and B; the velocity gradient is  $30 \text{ km s}^{-1}$  in 200 pc and the most blue-shifted  $H\alpha$  velocity has a smaller velocity than the H I velocity by about  $15 \text{ km s}^{-1}$ . The  $H\alpha$  velocity fields for NE, SE, NW, and SW are relatively calm.

### 3.2.4. *IC 2574*

The resultant six position-velocity diagrams are shown in Fig. 4. The width of the abscissa corresponds to  $200''$  or 2.9 kpc at IC 2574. This galaxy has a prominent H II complex in the northeastern part of the galaxy and this complex consists of several giant H II regions. Among them the observed positions cover the H II regions denoted as IC 2574-I and IC 2574-IV in Drissen *et al.* (1993); see Fig. 1 (c) and Table 2.

The  $H\alpha$  velocity crosses the H I velocity upward and downward on the position-velocity diagrams and the typical scale of the velocity variation is  $20 - 30 \text{ km s}^{-1}$  in 200 pc scale, which is similar to that observed at the outer regions in NGC 2363 as mentioned in Sec. 3.2.1. Unlike in NGC 2363, the  $H\alpha$  velocity field is chaotic at whole region of observed H II regions in IC 2574. Two V-shaped velocity features are prominent in the diagrams

for the slit positions B to D; the eastern (170'' to 140'') and the western (130'' to 100'') parts correspond to the H II regions IC 2574-IV and IC 2574-I, respectively. In IC 2574-I, the velocity gradient at the slit position D is steep, 50 km s<sup>-1</sup> in 400 pc, and the velocity difference between H $\alpha$  and H I at the most intense H $\alpha$  region is 20 km s<sup>-1</sup>. The line width is about 30 km s<sup>-1</sup>, a little larger than those in NGC 2366 and Holmberg II and rises to about 35 km s<sup>-1</sup> at the most H $\alpha$ -blue-shifted position in IC 2574-I, as shown in the diagrams for the slit positions B to D. Drissen *et al.* (1993) found three candidates of WR stars in IC 2574-I. The sharp edge of the velocity feature and the broad FWHM of the line in IC 2574-I seem to be related to the WR stars.

### 3.2.5. WLM

The resultant ten position-velocity diagrams are shown in Fig. 5. The width of the abscissa corresponds to 200'' or 0.9 kpc at WLM. As shown in Fig. 1 (d), the H II regions are in two blocks, the southern ring-shaped block and the northern barred-shaped block; hereafter we call them Southern ring and Northern bar, respectively (see Fig. 1 (d) and Table 2).

Both blocks of the H II regions are least luminous in the H $\alpha$  light among 13 observed H II regions. The velocity fields are flat and the calmest among four observed galaxies. The line widths are about 15 km s<sup>-1</sup>, which are smaller than those in other three observed galaxies. The slit positions D to F cross the hole of the Southern ring and an expanding shell-like feature is seen at  $-100''$  to  $-50''$  in the diagram for the slit position E.

## 4. Discussion

#### 4.1. Characteristics of the H $\alpha$ Position-Velocity Diagrams

We investigate characteristics of thirteen observed H II regions, the data of which are summarized in Table 2. We classify the morphologies of the H II regions into three types; the first is circular shape filled with H $\alpha$  emission, the second is ring shape, and the third is filament. We call them type-C, -R, and -F morphologies, respectively. Some H II regions with the type-F morphology seem to be a chain of small H II regions with the type-C morphology. The H $\alpha$  luminosities of the H II regions with the type-F morphology is less than  $2 \times 10^{38}$  erg s $^{-1}$ . We divide the type-C into two subgroups; type-C1 and C2 for H $\alpha$ -luminous ( $L(\text{H}\alpha) \geq 2 \times 10^{38}$  erg s $^{-1}$ ) one and H $\alpha$ -less luminous ( $L(\text{H}\alpha) < 2 \times 10^{38}$  erg s $^{-1}$ ) one, respectively.

The velocity features in the position-velocity diagrams are classified into four types and schematically shown in Fig. 6; we call them type-I, -II, -III, and -IV velocity features, respectively. The two classifications of the thirteen H II regions are listed in the last two columns of Table 5. Table 6 summarizes the classifications of thirteen H II regions as well as eight H II regions we previously observed in dwarf irregulars I Zw 36, Sextans A, NGC 6822, IC 1613, and NGC 1569 (Tomita *et al.* 1993, 1994). Table 6 shows that the morphological type and the velocity feature of the H II regions correlate well with each other; we characterize the H II regions into only five categories according to our classifications.

*Type-I and type-F or -C2:* The position-velocity diagrams for five less luminous H II regions from NGC 2366 NA to WLM Northern bar in Table 5 are flat. This is probably due to either lack of energetic stars which can generate strong wind or being at a young stage of evolution. IC 1613 S3, and probably IC 1613 S2 and Sextans A (the H II region at the eastern part of the galaxy) belong to this category (Tomita *et al.* 1993).

*Type-I and type-C1:* The velocity fields of powerful H II regions without sharp

velocity bumps suggest that the ages of the H II regions are too young to generate many evolved stars; examples are NGC 2366-III, Holmberg II NE and SE. At the central part of NGC 2363 the velocity field is flat, though it is chaotic at outer part. The velocity field which is calm in the central regions and chaotic at the outer regions in the luminous H II region is also observed in NGC 6822 HV (Tomita *et al.* 1993).

*Type-II and type-C1:* Roy *et al.* (1991) suggested that the ridge of the [O III] velocity field in NGC 2363, shown as a bump in the position-velocity diagrams at the positions NGC 2366 IA to ID (see Fig. 2 (a) and 2 (b)), is related to a chimney. I Zw 36, a well-studied blue compact dwarf galaxy, has type-II velocity feature (Tomita *et al.* 1994). Viallefond & Thuan (1983) gave the H $\beta$  flux of I Zw 36,  $f(\text{H}\beta) = 3.65 \times 10^{-13} \text{ erg s}^{-1} \text{ cm}^{-2}$ , and the distance of 4.6 Mpc. Assuming  $f(\text{H}\alpha)/f(\text{H}\beta) = 3$ , we get  $L(\text{H}\alpha) = 3 \times 10^{39} \text{ erg s}^{-1}$ . The relatively mild velocity field in spite of intense H $\alpha$  luminosity suggests the H II regions are at a young stage.

*Type-III and type-C1:* The V-shaped velocity feature associated to two H II regions in IC 2574 may indicate blow-out motions away from the galactic disk. The H II region HX in NGC 6822 also shows this kind of feature (Tomita *et al.* 1993).

*Type-III or -IV and type-R:* The H $\alpha$  ring shows an expanding bubble feature in the position-velocity diagrams; we discuss the kinematics following the analysis given by McCray & Cafatos (1987). The kinetic age of the bubble is  $t [\text{Myr}] = 0.6 (R/V)$  and the kinetic energy of the bubble is  $E [\text{erg}] = 1.3 \times 10^{42} R^3 V^2 n_0$ , where  $R$  is the radius in kpc,  $V$  is the expanding velocity in  $\text{km s}^{-1}$ , and  $n_0$  is the number density of the ambient interstellar matter in  $\text{cm}^{-3}$ . The number of supernova ( $N_{\text{SN}}$ ) responsible for the bubble kinetic energy is derived as  $N_{\text{SN}} = E / (0.2 \times 10^{51} \text{ erg})$  assuming that 20% of the supernova energy of  $10^{51} \text{ erg}$  contributes to the bubble kinetic energy. Though we did not observe whole regions of Holmberg II Center, we take the expanding velocity for Holmberg II Center as  $30 \text{ km s}^{-1}$

from the data at the position-velocity diagram for the position A. With a radius of 200 pc, we get  $t = 4$  Myr,  $E = 1 \times 10^{52}$  erg, and  $N_{\text{SN}} = 50$ , assuming  $n_0 = 1 \text{ cm}^{-3}$ . The bubble feature seen in the position NGC 2366 SB has the same radius and expanding velocity as those for Holmberg II Center; 200 pc and  $30 \text{ km s}^{-1}$ , respectively. Hunter *et al.* (1993) pointed out a possible connection between the H $\alpha$  filamentary structure around NGC 2363 and the extraordinary high velocity feature claimed by Roy *et al.* (1991). The bubble feature seen at NGC 2366 SB corresponds to a part of the H $\alpha$  filament (see Fig. 1(a) and mentioned in Sec.3.2.1), therefore, this filament was generated by a local bubble, off the central part of NGC 2363. WLM Southern ring has a radius of 150 pc and an expanding velocity of  $20 \text{ km s}^{-1}$ . Then,  $t = 4.5$  Myr,  $E = 2 \times 10^{51}$  erg, and  $N_{\text{SN}} = 10$  are obtained, assuming  $n_0 = 1 \text{ cm}^{-3}$ . The age derived is consistent with the result by Ferraro *et al.* (1989) that the star formation stopped a few Myr ago in the region including this H II region (denoted as Region 2 by them).  $N_{\text{SN}}$  is similar to those for expanding shells in NGC 1569 (denoted as SS's in Tomita *et al.* 1994). The bubbles in our sample have much larger  $N_{\text{SN}}$  than those observed by Oey & Massey (1994) in M 33.

Puche *et al.* (1992) found many H I holes in Holmberg II. Puche *et al.* (1992), Mashchenko & Silich (1995), and Tongue & Westpfahl (1995) argued that they are cavities generated by the star formation activity, and Hunter *et al.* (1993) claimed a possibility that the holes were made by the penetration of the high velocity clouds because the H $\alpha$  emission does not encircle the H I holes as is the case in LMC which is expected for cavities by violent star formation. We do not detect the expanding-bubble velocity features for the H II regions which surround the H I holes in Holmberg II as we observe in WLM. Our data does not support the idea that the star formation cavities are responsible for the H I holes in Holmberg II.



## 4.2. Comparison of the Velocity Field between H $\alpha$ and H I

The FIR-to- $B$  luminosity ratio,  $L_{FIR}/L_B$ , is an indicator of the present star formation activity of the galaxy per luminous mass (Tomita *et al.* 1996). The ratios are 0.3, 0.2, 0.05, and 0.01 for IC 2574, NGC 2366, Holmberg II, and WLM, respectively (see Table 1); the activity ranges over 1.5 order of magnitude. The ratio of the H I mass to  $B$ -band luminosity ( $M_{HI}/L_B$ ), on the other hand, are about 0.1 for all four galaxies (see Table 1). Huchtmeier *et al.* (1981) presented H I extents for Holmberg II, NGC 2366, and WLM. At a level of  $10^{19}$  cm $^{-2}$  of the H I column density, the radii of the H I extent are 27', 30', and 45', respectively, and these correspond to 3.3, 3.6, and 3.8 times the Holmberg radius, respectively; the H I to optical size ratios are similar to each other among the three galaxies. The average H I surface densities are several to ten times  $10^5 M_{\odot}$  kpc $^{-2}$  and are also similar to each other among the three galaxies. No correlation between the star formation activity, such as  $L_{FIR}/L_B$ , and the H I density suggests that some external causes or internal but intermittent causes trigger the generation of the star forming regions as well as cloud formation by the self gravity or shell sweeping (e.g., Oey & Massey 1995).

Saitō *et al.* (1992) proposed a model based on observed H $\alpha$  and H I velocity fields of IC 10 that infalling clouds from the extended H I envelope of the galaxy may cause the intense star formation. In their model, the H II regions made by infalling H I clouds have bulk motions of about 10 km s $^{-1}$  relative to the ambient H I disk. The chaotic velocity fields, with bubbles or blow-out features through the intense star formation, presented by types-III and IV, would disturb the information about the original bulk motion of star-forming clouds. On the other hand, the calm H $\alpha$  velocity field, types-I and II, is suitable to measure the original bulk motion of the H II regions. We investigate eight H II regions; NGC 2363 (the slit position of NGC 2366 SG), NGC 2366-III (the slit position of NGC 2366 SD), NGC 2366 NA, NGC 2366 ND, Holmberg II NE, SE, NW, and SW.

Table 7 lists the H I and H $\alpha$  radial velocities as well as the velocity difference between them. In three out of eight, NGC 2363, Holmberg II NE, and Holmberg II NW, we detect a little or no velocity difference. In other three H II regions in NGC 2366, we detect velocity differences of about 10 km s<sup>-1</sup>. We detect velocity differences of 15 to 20 km s<sup>-1</sup> for other two H II regions in Holmberg II. The distribution of the velocity differences among the eight H II regions ranges  $-10$  km s<sup>-1</sup> to 20 km s<sup>-1</sup> and the average is several km s<sup>-1</sup>. In the previous study by Tomita *et al.* (1993), five H II regions, I Zw 36, Sextans A, IC 1613 S2 and S3, and NGC 6822 HV, in four galaxies have type-I or -II velocity features (see Table 6). Fig. 7 summarize in histogram the observed velocity differences of H $\alpha$  – H I for H II regions with type-I or -II velocity features including above five H II regions. The standard deviation of the velocity difference is about 5 km s<sup>-1</sup>, which is consistent with the expectation from the model by Saitō *et al.* (1992). Though it is marginal and it is not conclusive because such a velocity difference may be generated by internal motion through star formation activity, this suggests that some of the H II regions in dwarf irregulars formed through the infall of clouds onto the galactic disk. Search for high velocity clouds around the galaxies are needed to confirm this hypothesis.

We would like to thank Yoh-ichi Kanamori for his help with the observations, and the OAO staff members for their hospitality during our stay. T.T.T. acknowledges the Research Fellowship of the Japan Society for the Promotion of Science for Young Scientists. Finally, we are grateful to the anonymous referee for improving the paper.

## REFERENCES

- Ables, H.D., & Ables, P.G. 1977, *ApJS*, 34, 245
- Arsenault, R., & Roy, J.-R. 1986, *AJ*, 92, 567
- Braun, R. 1995, *A&AS*, 114, 409
- de Vaucoulerus, G., de Vaucoulerus, A., Corwin, H.G., Jr., Buta, R.J., Paturel, G., & Forqué, P. 1991, *Third Reference Catalogue of Bright Galaxies* (Springer-Verlag, New York)
- Drissen, L., Roy, J.-R., & Moffat, A.F.J. 1993, *AJ*, 106, 1460
- Ferraro, F.R., Pecci, F.F., Tosi, M., & Buonanno, R. 1989, *MNRAS*, 241, 433
- González-Delgado, R.M., Pérez, E., Tenorio-Tagle, G., Vilchez, J.M., Terlevich, E., Terlevich, R., Telles, E., Rodríguez-Espinosa, J.M. *et al.* 1994, *ApJ*, 437, 239
- Hodge, P., & Miller, B.W. 1995, *ApJ* 451, 176
- Hodge, P., Strobel, N.V., & Kennicutt, R.C. 1994, *PASP*, 106, 309
- Horaguchi, T., Ichikawa, S., Yoshida, M., Yoshida, S., & Hamabe, M. 1994, *Publ. Natl. Astron. Obs. Jpn*, 4, 1
- Huchtmeier, W.K., Seiradakis, J.H., & Materne, J. 1981, *A&A*, 102, 134
- Hunter, D.A., & Gallagher, III, J.S. 1986, *PASP*, 98, 5
- Hunter, D.A., Hawley, W.N., & Gallagher, III, J.S. 1993, *AJ*, 106, 1797
- Hunter, D.A., & Sage, L. 1993, *PASP*, 105, 374
- Kennicutt, R., Balick, B., & Heckman, T. 1980, *PASP*, 92, 134

- Kosugi, G., Ohtani, H., Sasaki, T., Koyano, H., Shimizu, Y., Yoshida, M., Sasaki, M., Aoki, K., & Baba, A. 1995, *PASP*, 107, 474
- Martimbeau, N., Carignan, C., & Roy, J.-R. 1994, *AJ*, 107, 543
- Mashchenko, S. Ya., & Silich, S.A. 1995, *Astronomy Reports*, 39, 587
- Mayya, Y.D. 1994, *AJ*, 108, 1276
- McCray, R., & Kafatos, M. 1987, *ApJ*, 317, 190
- Miller, B.W., & Hodge, P. 1994, *ApJ*, 427, 656
- Oey, M.S., & Massey, P. 1994, *ApJ*, 425, 635
- Oey, M.S., & Massey, P. 1995, *ApJ*, 452, 210
- Puche, D., Westpfahl, D., Brinks, E., & Roy, J.-R. 1992, *AJ*, 103, 1841
- Rice, W., Lonsdale, C.J., Soifer, B.T., Neugebauer, G., Kopan, E.L., Lloyd, L.A., de Jong, T., & Habing, H.J. 1988, *ApJS*, 68, 91
- Roy, J.-R., Boulesteix, J., Joncas, G., & Grundseth, B. 1991, *ApJ*, 367, 141
- Roy, J.-R., Aubé, M., McCall, M.L., & Dufour, R.J. 1992, *ApJ*, 386, 498
- Saitō, M., Sasaki, M., Ohta, K., & Yamada, T. 1992, *PASJ*, 44, 593
- Sandage, A., & Carlson, G. 1985, *AJ*, 90, 1464
- Takata, T., Ichikawa, S., Horaguchi, T., Yoshida, S., Yoshida, M., Ito, T., Nishihara, E., & Hamabe, M. 1995, *Publ. Natl. Astron. Obs. Jpn*, 4, 9
- Terlevich, R., & Melnick, J. 1981, *MNRAS*, 195, 839
- Tolstoy, E., Saha, A., Hoessel, J.G., & McQuade, K. 1995, *AJ*, 110, 1640

Tomita, A., Ohta, K., & Saitō, M. 1993, PASJ, 45, 693

Tomita, A., Ohta, K., & Saitō, M. 1994, PASJ, 46, 335

Tomita, A., Tomita, Y., & Saitō, M. 1996, PASJ, 48, 285

Tongue, T.D., & Westpfahl, D.J. 1995, AJ, 109, 2462

Viallefond, F., & Thuan, T.X. 1983, ApJ, 269, 444

Wevers, B.M.H.R., van der Kruit, P.C., & Allen, R.J. 1986, A&AS, 66, 505

Fig. 1.— The slit positions superimposed on the H $\alpha$  images. The length of each line corresponds to the length of the abscissa of Fig. 2. (a) NGC 2366: the H $\alpha$  image is taken from Roy *et al.* (1991)’s Fig. 1. The length of the line corresponds to 160". (b) Holmberg II: the H $\alpha$  image is taken from Hodge *et al.* (1994)’s Fig. 1. The length of the line corresponds to 250". (c) IC 2574: the H $\alpha$  image is taken from Miller & Hodge (1994)’s Fig. 3. The length of the line corresponds to 200". (d) WLM: the H $\alpha$  image is taken from Hodge & Miller (1995)’s Fig. 1 (a). The length of the line corresponds to 200".

Fig. 2.— Position-velocity diagrams for NGC 2366 (Fig. 2 (a) – 2 (h)). Sixteen panels are presented and the slit position name is labeled at the top of each panel. The abscissa indicates the position along the slit in arcsec and the coordinates of the origin is listed in Table 4. The ordinate indicates the heliocentric radial velocity and the FWHM of the H $\alpha$  emission line. A filled circle indicates the central velocity of the line and an open circle indicates the FWHM of the line. The scales for the central velocity and the FWHM of the line are shown in the left-side and the right-side ordinates, respectively. The horizontal and vertical error bars on a filled circle show the binning width and the error of measurement of the central velocity, respectively. The instrumental broadening is reduced from the observed line width to derive the FWHM. The dotted line shows the 0 km s $^{-1}$ -level for the FWHM. The thick curve indicates the H I velocity. The data is taken from Wevers *et al.* (1986). The cross in the upper-left corner of the panel shows the accuracy of the H I observations. The full length of the horizontal line of the cross, 24", indicates the FWHM of the beam for the H I isovelocity map. For four positions of NGC 2366 IA to ID, the FWHM is 25", since the size of the beam depends on the position angle. The half length of the vertical line of the cross, 8.25 km s $^{-1}$ , indicates the channel spacing of the H I observations.

Fig. 3.— The same as Fig. 2 but for Holmberg II. The H I data is taken from Puche *et al.* (1992). The beam size and the channel spacing of the H I observations are 4.5" and

2.58 km s<sup>-1</sup>, respectively.

Fig. 4.— The same as Fig. 2 but for IC 2574. The H I data is taken from Martimbeau *et al.* (1994). The beam size and the channel spacing of the H I observations are 30'' and 8.24 km s<sup>-1</sup>, respectively.

Fig. 5.— The same as Fig. 2 but for WLM. There is no synthetic H I observations in literature so far.

Fig. 6.— Schematic pictures of four types of the velocity features in the position-velocity diagram. In ordinate, the upper direction indicates larger recession velocity. The type is shown in the upper right corner in each panel.

Fig. 7.— Histogram of the bulk motion of the H II regions relative to the galactic H I disk defined by H $\alpha$  – H I. The data for thirteen H II regions with type-I or -II velocity feature including the samples observed by Tomita *et al.* (1993) are presented.

TABLE 1: Basic characteristics of the observed galaxies.

(1)	(2)	(3)	(4)	(5)	(6)	(7)	(8)	(9)
Name	Distance	Size	$i$	$\log f_{FIR}$	$L_{FIR}$	$L_B$	$M_T$	$M_{HI}$
	[Mpc]	[kpc]	[ $^\circ$ ]	[ $\log \text{W m}^{-2}$ ]	[ $10^8 L_\odot$ ]	[ $10^8 L_\odot$ ]	[ $10^9 M_\odot$ ]	[ $10^9 M_\odot$ ]
NGC 2366	3.44	8.3	65	- 12.57	1.00	4.6	3	0.5
Holmberg II	3.2	7.5	47	- 13.15	0.23	4.3	2	0.7
IC 2574	3.0	11.7	77	- 12.67	1.70	6.2	8	0.6
WLM	0.97	3.3	69	- 13.63	0.007	0.5	1	0.06

Columns:

(1) Name of the galaxy. (2) Distance taken from literature; for NGC 2366 Tolstoy *et al.* (1995), for Holmberg II Puche *et al.* (1992), for IC 2574 Martimbeau *et al.* (1994), and for WLM Sandage & Carlson (1985). (3) Physical size corresponding to the diameter  $D_0$  given in de Vaucouleurs *et al.* (1991). (4) Apparent inclination of the galaxy taken from literature; for NGC 2366 Wevers *et al.* (1986), for Holmberg II Puche *et al.* (1992), for IC 2574 Martimbeau *et al.* (1994), and for WLM Ables & Ables (1977). (5) Far-infrared ( $42.5 - 122.5 \mu\text{m}$ ) flux calculated from flux densities at  $60 \mu\text{m}$  and  $100 \mu\text{m}$  measured by *IRAS*. Sources: for NGC 2366 X0723+693 from Small Scale Structure Catalog, for Holmberg II F08140+7052 from Faint Source Catalog, and for IC 2574 and WLM from the data given by Rice *et al.* (1988). (6) Far-infrared luminosity. (7)  $B$  band luminosity. (8) Dynamical total mass of the galaxy derived from the H I observations taken from literature; for NGC 2366 Wevers *et al.* (1986), for Holmberg II Puche *et al.* (1992), for IC 2574 Martimbeau *et al.* (1994), and for WLM Huchtmeier *et al.* (1981). Huchtmeier *et al.* (1981) adopted 1.6 Mpc as the distance to WLM and we converted the value for 0.97 Mpc. (9) The H I mass of the galaxy.



TABLE 2: Characteristics of the observed H II regions.

Galaxy (1)	H II region (2)	Other ID (3)	$f(\text{H}\alpha)$ (4)	Mor. (5)	$\Sigma f(\text{H}\alpha)$ (6)	$L(\text{H}\alpha)$ (7)	Ref	Note					
NGC 2366	NGC 2363	NGC 2366-I,II	6710	b	6710	95	1,2	(i)					
	NGC 2366-III		1000	b	1000	14		(ii)					
	NGC 2366 NA		100	b	100	1.4		(iii)					
	NGC 2366 ND		100	b	100	1.4		(iii)					
Holmberg II	NE	Hodge	71	159	b	593	7.3	3					
			73	339	l								
			74	95	b								
	SE	Hodge	70	244	c	244	3.0	3					
	Center	Hodge	45	754	b,c,l	754	9.2	3					
	NW	Hodge	16	42.6	b	103	1.3	3					
			17	60.3	b								
	SW	Hodge	18	19.0	f	90	1.1	3					
			20	71.1	b								
	IC 2574	IC 2574-I	Hodge	167	502.93	b	1095	12	4	(iv)			
169				313.54	b								
179				79.29	b								
180				108.99	b								
185				90.43	b								
IC 2574-IV		Hodge	194	191.08	b	487	5.3	4	(iv)				
			198	167.04	b								
			202	129.13	b								
WLM	Northern bar	Hodge	2	52.74	b	318	0.4	5					
			3	13.68	f								
			4	40.72	b								
			5	9.22	f								
			8	54.44	b								
			9	107.79	b								
			13	9.44	f								
			14	10.29	f								
			15	19.88	f								
			Southern ring	Hodge	6				45.54	b	299	0.3	5
					7				159.23	b			
			10	10.86	f								
		11	37.54	b									
		12	45.86	f									

Columns:

(1) Galaxy name. (2) Name of the H II regions in this paper. (3) Name of individual H II regions in other papers mainly by Hodge and his collaborators which are here denoted as ‘Hodge #’. (4) Flux of the  $\text{H}\alpha$ ; the reference is shown in the eighth column. The unit is  $10^{-15} \text{ erg s}^{-1} \text{ cm}^{-2}$ . (5) Hodge-type morphology; c: compact, b: bright compact, f: faint compact, l: loops or rings, and d: diffuse emission. (6) Total flux of the  $\text{H}\alpha$  summing up the values in the fourth column. The unit is  $10^{-15} \text{ erg s}^{-1} \text{ cm}^{-2}$ . (7) Luminosity of the  $\text{H}\alpha$  in the unit of  $10^{38} \text{ erg s}^{-1}$ .

References:

(1) Mayya (1994); (2) Kennicutt *et al.* (1980); (3) Hodge *et al.* (1994); (4) Miller & Hodge (1994); (5) Hodge & Miller (1995)

NOTES:

(i) We combine NGC 2366-I and II as NGC 2363 because of close position, though originally NGC 2363 corresponds to NGC 2366-I. We derive the  $H\alpha$  flux using values  $\log f(H\alpha + [N II]) [\text{erg s}^{-1}\text{cm}^{-2}] = -11.16$  given by Mayya (1994) for the H II region with ID '1 + 2', and  $[N II]/H\alpha \sim 0.03$  given by Kennicutt *et al.* (1980). We give the morphology following Hodge's classification. Note that NGC 2363 can be divided into many small H II regions.

(ii) We estimate the  $H\alpha$  flux considering that the surface brightness and area are 0.6 and 0.25 of those for NGC 2363, respectively. We give the morphology following Hodge's classification. Note that NGC 2366-III can be divided into many small H II regions.

(iii) We estimate the  $H\alpha$  flux considering that the surface brightness and area are 0.25 and 1/15 of those for NGC 2363, respectively. We give the morphology following Hodge's classification.

(iv) Martimbeau *et al.* (1994) reported that  $f(H\alpha) [\text{erg s}^{-1}\text{cm}^{-2}] = 7.8 \times 10^{-13}$  and  $4.7 \times 10^{-13}$  for IC 2574-I and IV, respectively.

TABLE 3: Log of the observations.

(1)	(2)	(3)	(4)
1994			csd
Jan 11	T, O	Holmberg II, IC 2574	10494, 10496, 10497
13	T, O	Holmberg II, IC 2574	10503, 10508
Dec 3	T, N, K	NGC 2366	13163, 13164, 13168
4	T, O, N, K	WLM	13177
5	O, N, K	NGC 2366, WLM	13185, 13186, 13187, 13189, 13192
6	O, N, K	NGC 2366, WLM	13201, 13202, 13203, 13209, 13210

Columns:

(1) Date in 1994. (2) Observers: T: Akihiko Tomita, O: Kouji Ohta, N: Kouichiro Nakanishi, K: Yoh-ichi Kanamori. (3) Objects observed. (4) Frame ID-numbers of objects used in our paper. Real frame name is like csd10494.001 and here we omit the prefix of 'csd' and the extension which consists of three numbers.

NOTE:

You can see the quick looks of the raw data of our observations through Mitaka-Okayama-Kiso data Archival system (MOKA). See <http://www.moka.nao.ac.jp>. The MOKA is operated by Astronomical Data Analysis Center, Okayama Astrophysical Observatory (National Astronomical Observatory of Japan), and Kiso observatory (University of Tokyo) in cooperation with the Japan Association Information Processing in Astronomy (Horaguchi *et al.* 1994; Takata *et al.* 1995).

TABLE 4: Observed slit positions.

(1)	(2)	(3)	(4)	(5)	(1)	(2)	(3)	(4)	(5)
	h m s	° ' "	°	csd		h m s	° ' "	°	csd
NGC 2366					IC 2574				
IA	07 23 25.0	+ 69 17 29	45	13163.002	A	10 25 40.5	+ 68 43 56	90	10497.002
IB	07 23 24.2	+ 69 17 33	45	13163.005	B	10 25 40.5	+ 68 43 50	90	10497.005
IC	07 23 23.4	+ 69 17 37	45	13164.001	C	10 25 40.5	+ 68 43 44	90	10497.008
ID	07 23 22.6	+ 69 17 42	45	13168.004	D	10 25 40.5	+ 68 43 38	90	10508.003
SA	07 22 59.1	+ 69 17 58	90	13187.005	E	10 25 40.5	+ 68 43 32	90	10508.006
SB	07 22 59.1	+ 69 17 52	90	13187.008	F	10 25 40.5	+ 68 43 26	90	10508.012
SC	07 22 59.1	+ 69 17 46	90	13187.011	WLM				
SD	07 22 59.1	+ 69 17 40	90	13189.002	A	23 59 24.0	- 15 45 37	0	13177.001
SE	07 22 59.1	+ 69 17 34	90	13189.005	B	23 59 23.6	- 15 45 37	0	13177.004
SF	07 22 59.1	+ 69 17 31	90	13202.004	C	23 59 23.2	- 15 45 37	0	13201.004
SG	07 22 59.1	+ 69 17 28	90	13202.007	D	23 59 22.7	- 15 45 37	0	13185.008
SH	07 22 59.1	+ 69 17 25	90	13203.001	E	23 59 22.3	- 15 45 37	0	13201.007
NA	07 23 10.8	+ 69 20 10	90	13209.001	F	23 59 21.9	- 15 45 37	0	13186.002
NB	07 23 10.8	+ 69 20 01	90	13192.003	G	23 59 21.5	- 15 45 37	0	13201.013
NC	07 23 10.8	+ 69 19 45	90	13210.004	H	23 59 21.1	- 15 45 37	0	13186.005
ND	07 23 10.8	+ 69 19 06	90	13210.007	I	23 59 20.7	- 15 45 37	0	13201.016
Holmberg II					J	23 59 20.2	- 15 45 37	0	13201.019
A	08 14 05.6	+ 70 52 26	90	10494.002					
B	08 14 05.6	+ 70 52 20	90	10494.005					
C	08 14 05.6	+ 70 52 14	90	10496.001					
D	08 14 05.6	+ 70 52 08	90	10496.007					
E	08 14 05.6	+ 70 52 02	90	10196.010					
F	08 14 05.6	+ 70 51 56	90	10503.004					
G	08 14 05.6	+ 70 51 50	90	10503.007					

Columns:

(1) Position ID name. (2) Right ascension of the origin point of the slit position in 1950.0 equinox. (3) Declination of the origin point of the slit position in 1950.0 equinox. (4) Position angle of the slit. (5) Frame ID-number used. We omit the prefix 'csd'.

TABLE 5: Classification of the observed H II regions.

H II region	$L(\text{H}\alpha)$ [ $10^{38} \text{erg s}^{-1}$ ]	Mor.	Vel.
NGC 2363	95	C	II
NGC 2366-III	14	C	I
IC 2574-I	12	C	III
Holmberg II Center	9.2	C,R	III
Holmberg II NE	7.3	C	I
IC 2574-IV	5.3	C	III
Holmberg II SE	3.0	C	I
NGC 2366 NA	1.4	C	I
NGC 2366 ND	1.4	C	I
Holmberg II NW	1.3	F	I
Holmberg II SW	1.1	C	I
WLM Northern bar	0.4	F	I
WLM Southern ring	0.3	R	IV

TABLE 6: Classification of the H II regions.

MORPH.	Filamentary	Circular (less luminous)	Circular (luminous)	Ring
VEL. FEATURE	(F)	(C2)	(C1)	(R)
Flat (I)	Ho II NW	N2366 NA	N2366-III	
	WLM N-Bar	N2366 ND	Ho II NE	
	I1613 S3	Ho II SW	Ho II SE	
	(I1613 S2?)	(Sex A?)	N6822 HV	
Upper-bumpy (II)			N2363 I Zw 36 (N1569 Arcs?)	
	Vally-like (III)		I2574-I I2574-IV N6822 HX (N1569 Arcs?)	
Circular split (IV)			Ho II Center <sup>a</sup> N1569 SS's <sup>a</sup>	
				WLM S-Ring

<sup>a</sup> The morphology is between type-C1 and type-R.

TABLE 7: Velocity differences between H I and H $\alpha$ .

H II region	H I [km s <sup>-1</sup> ]	H $\alpha$ [km s <sup>-1</sup> ]	H $\alpha$ - H I [km s <sup>-1</sup> ]
NGC 2363	80 $\pm$ 8	80	$\pm$ 0
NGC 2366-III	70 $\pm$ 8	60	- 10
NGC 2366 NA	130 $\pm$ 8	141	+ 11
NGC 2366 ND	120 $\pm$ 8	130	+ 10
Holmberg II NE	157 $\pm$ 3	152	- 5
Holmberg II SE	157 $\pm$ 3	175	+ 18
Holmberg II NW	156 $\pm$ 3	160	+ 4
Holmberg II SW	156 $\pm$ 3	170	+ 14